

5-7-2011

Expression Analysis of the Imprinted Gene Transketolase-like 1 in Mouse and Human

Amy F. Friss

University of Connecticut - Storrs, amy.friss@gmail.com

Recommended Citation

Friss, Amy F, "Expression Analysis of the Imprinted Gene Transketolase-like 1 in Mouse and Human" (2011). *Master's Theses*. 90.
https://opencommons.uconn.edu/gs_theses/90

This work is brought to you for free and open access by the University of Connecticut Graduate School at OpenCommons@UConn. It has been accepted for inclusion in Master's Theses by an authorized administrator of OpenCommons@UConn. For more information, please contact opencommons@uconn.edu.

Expression Analysis of the Imprinted Gene *Transketolase-like 1* in Mouse and Human

Amy Frances Friss

University of Connecticut

Abstract

Genomic imprinting is an epigenetic phenomenon resulting in differential gene expression based on parental origin. Recently, *transketolase-like 1* (*TKTL1*) has been identified as an X-linked imprinted gene. *TKTL1* functions in the nonoxidative branch of the pentose phosphate pathway (PPP), which maintains glutathione in a reduced state through the generation of NADPH. Previous studies on transaldolase, the other critical enzyme in the nonoxidative branch of the PPP, suggest that *TKTL1* may affect the cell's ability to reduce glutathione. This study provides evidence that *TKTL1* overexpression inhibits glutathione reduction. Intriguingly, aberrant glutathione levels are associated with autism. Additionally, studies involving Turner syndrome females found that differences in social behavior could distinguish females expressing the maternal X chromosome from those expressing the paternal X chromosome. This led researchers to hypothesize the influence of an X-linked imprinted gene in autism. Accordingly, this study compared *TKTL1* expression levels in autistic patients versus their unaffected siblings. The results suggest that further studies are required.

Expression Analysis of the Imprinted Gene *Transketolase-like 1* in Mouse and Human

Amy Frances Friss

B.S., University of Connecticut, 2009

A Thesis

Submitted in Partial Fulfillment of the

Requirements for the Degree of

Master of Science

At the

University of Connecticut

2011

APPROVAL PAGE

Master of Science Thesis

Expression Analysis of the Imprinted Gene *Transketolase-like 1* in Mouse and Human

Presented by

Amy Frances Friss, B. S.

Major Advisor _____
Michael O'Neill, Ph.D.

Associate Advisor _____
Rachel O'Neill, Ph.D.

Associate Advisor _____
Barbara Mellone, Ph.D.

University of Connecticut

2011

ACKNOWLEDGEMENTS

Thank you to everyone who has provided guidance and advice throughout my graduate studies. I would especially like to thank my advisor, Dr. Michael O'Neill, for allowing me the opportunity to join his lab as an undergraduate and continue on for my graduate research. My experiences in your lab have not only taught me how to perform techniques, but they have taught me the importance of ethical research and scientific integrity. I have learned more in your lab than I could have imagined. Thank you to my committee members, Dr. Rachel O'Neill and Dr. Barbara Mellone, for all of the help that you have provided and all that you have taught me.

I would like to thank Inga for training me and for being a wonderful mentor; what I have learned from you is invaluable. Thank you to Seth, Mike, Sohaib, Rob and Nate for always answering my questions and for helping me whenever I needed it. I would also like to thank Judy for providing assistance with my cell culture, it was an immense help. Thank you to everyone in Beach Hall for making graduate school a wonderful and unforgettable experience.

Thank you to my friends, my boyfriend J.R. and my family, all of whom have been very supportive and understanding. I would especially like to thank my dad and my sister. Dad, you have always been there for me and I appreciate it more than I can say. Tracey, my sister and my best friend, you have been there to listen to me, advise me and share my experiences with me. No words can express what this means to me. I would finally like to thank my mom; I know you are always watching over me and for that I am eternally grateful.

TABLE OF CONTENTS

Chapter 1: Background Information.....	1
1.1 Epigenetics and Imprinting.....	1
1.2 X-Linked Imprinting.....	4
1.3 Search for X-Linked Imprinted Genes.....	6
Chapter 2: <i>TKTL1</i> Overexpression Studies.....	8
2.1 Background Information.....	8
Pentose Phosphate Pathway.....	8
<i>Transketolase-like 1</i>	11
2.2 Overexpression Studies.....	12
Construct Formation.....	13
Transfection.....	13
Western Blot Analysis.....	18
<i>TKTL1</i> Expression Analysis.....	20
Glutathione Assay.....	21
Glutathione Assay Results.....	22
Glutathione Assay Analysis.....	26
NADPH Experiments.....	26
NADPH Assay Results.....	26
NADPH Assay Analysis.....	27
<i>G6pdx</i> Expression.....	28
<i>G6pdx</i> Expression Analysis.....	28

Discussion.....	29
Chapter 3: Human Lymphoblast Autism Studies.....	30
3.1 Background Information.....	30
Autism.....	30
Turner Syndrome and Skuse Hypothesis.....	32
3.2 Human Lymphoblast Studies.....	33
<i>TKTL1</i> Expression Results.....	34
<i>TKTL1</i> Expression Analysis.....	39
Discussion.....	40
Chapter 4: Synopsis.....	44
Chapter 5: Methods.....	45
Protocol 1: <i>TKTL1</i> Expression Construct Formation.....	45
Protocol 2: Expression of <i>TKTL1</i>	45
Protocol 3: Western Blot.....	46
Protocol 4: Total RNA Extraction.....	46
Protocol 5: Real-Time RT-PCR.....	46
Protocol 6: Glutathione Assay.....	47
Protocol 7: NADP ⁺ /NADPH Assay.....	47
Protocol 8: Human Lymphoblastoid Cell Culture.....	48
Protocol 9: Human Lymphoblastoid Real-Time RT-PCR.....	48
Chapter 6: Supplemental Information.....	50
Chapter 7: References.....	65

Chapter 1: Background Information

1.1 Epigenetics and Imprinting

Genomic imprinting is an epigenetic phenomenon resulting in parent-of-origin gene expression. Epigenetic mechanisms mediate genomic imprinting, leaving the DNA sequence unchanged. These mechanisms primarily include DNA methylation patterns and histone modifications. The epigenetic marking of an imprinted gene's alleles designate their parental origin, allowing for appropriate expression patterns in the soma¹.

Differential DNA methylation is the hallmark of imprinted genes. A differentially methylated region (DMR) is only methylated on one parental allele, typically on the cytosine of CpG dinucleotides². Often, DMRs constitute imprinting control regions (ICRs)². The imprint is established in the germline and is maintained throughout genome-wide demethylation during preimplantation development¹. Deletion of an imprinted gene's ICR can result in loss of imprinted gene expression or reversion to biallelic expression¹.

DNA methylation is regulated by DNA methyltransferases (DNMTs), which are classified as *de novo* methyltransferase or maintenance methyltransferase. DNMT3A and DNMT3B are the *de novo* methyltransferases, assisted by the DNMT3L protein. Though it is homologous to DNMT3A and DNMT3B, DNMT3L has no catalytic activity³ but is still a regulator of imprint establishment⁴. Research demonstrated DNMT3L association with DNMT3A only in species in which imprinting occurs, suggesting that DNMT3L acquisition may have been related to the evolution of imprinting.⁵ Together, DNMT3A and DNMT3L are responsible for *de novo* methylation of most ICRs. Hemimethylated

DNA is methylated by DNMT1, the enzyme necessary for maintaining DNA methylation at imprinted loci and across the genome.

Histones exhibit post-translational modifications including methylation and acetylation. Methylation of specific amino acid residues occurs via histone methyltransferase. Actively transcribing regions are typically methylated on arginine residues whereas methylation of lysine (K) residues is typically associated with repression, except for H3K4 trimethylation⁶ and H4K20 monomethylation⁷ which result in active transcription. Histones are acetylated or deacetylated using histone acetyltransferase (HAT) or histone deacetylase (HDAC), respectively. Upon acetylation, chromatin is transformed into a more relaxed structure that is associated with more actively transcribing DNA. The acetyl group carries a negative charge that interacts with the positively charged histones to create a neutral environment. A neutral environment decreases the histones' interaction with the negatively charged DNA, providing greater accessibility for transcription factors.

Chromatin packages DNA into a structure that fits into the cell and is strong for support during mitosis and meiosis. Chromatin is composed of histone octamers, dimers of subunits H2A, H2B, H3 and H4, wrapped in DNA, forming a nucleosome⁸. The different states of chromatin control gene expression and DNA replication: heterochromatin is associated with non-transcribing regions; euchromatin with actively transcribing regions.

Imprinted genes are generally found in 1Mb clusters controlled by one ICR¹. Clusters are typically regulated in one of two ways, including use of an insulator to control access to the shared regulatory elements of the cluster and silencing of the cluster

by noncoding RNA (ncRNA)¹. The *H19/Igf2* locus is controlled by the insulator mechanism, while ncRNA regulates the *Igf2r* cluster in mouse⁹.

H19 is a paternally imprinted (maternally expressed) gene on mouse chromosome 7, coding for a 2.2Kb non-coding RNA¹⁰. *Insulin-like growth factor 2 (Igf2)* is a maternally imprinted (paternally expressed)^{11,12} gene influencing fetal growth and is found within the same cluster as *H19*. Both genes share an enhancer¹³ and are controlled by the same ICR^{14,15}. On the maternal allele the ICR binds CTCF, a protein that mediates insulator activity at the β -globin locus¹⁶. CTCF binding blocks interaction of *Igf2* with the enhancers, while *H19* retains access and proceeds with transcription¹⁷. The ICR is methylated on the paternal allele, blocking CTCF binding and preventing *H19* from interacting with the enhancers while *Igf2* maintains interaction⁹ (Figure 1.1).

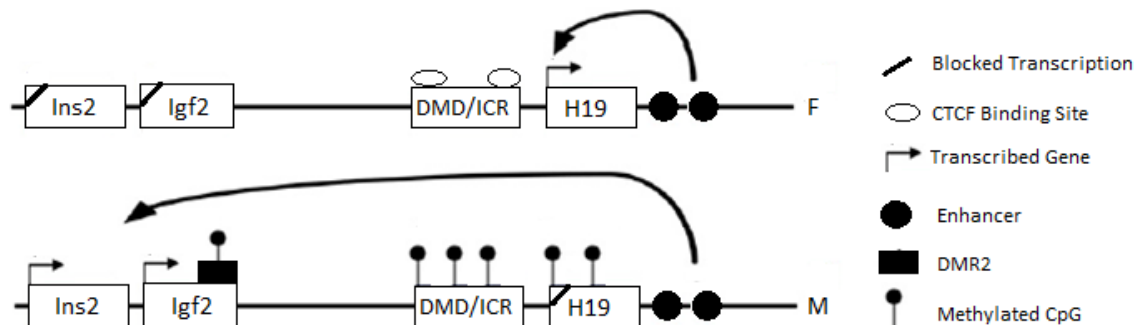


Figure 1.1 Imprinted *H19/Igf2* cluster. Figure adapted from Bartolomei et al¹.

More commonly, ncRNAs appear to regulate imprinting in clusters¹⁸, as in the *insulin-like growth factor 2 receptor (Igf2r)* cluster on mouse chromosome 17A¹⁹ (Figure 1.2). The *Igf2r* cluster consists of maternally expressed genes *Igf2r*, solute carrier 22a2 and 22a3 (*Slc22a22* and *Slc22a3*, respectively), paternally expressed antisense *Igf2r*

RNA (*Airn*) and a few non-imprinted genes. *Airn* is a 108 kb ncRNA that is arranged in an antisense orientation to *Igf2r*, with its promoter located in the cluster's ICR¹. On the maternal chromosome the ICR is hypermethylated, preventing *Airn* transcription but allowing transcription of *Igf2r*, *Slc22a22* and *Slc22a3*. On the paternal copy, the ICR is unmethylated; however the *Igf2r* promoter is methylated after transcription initiation of the imprinted gene. *Igf2r* promoter methylation leads to transcription of *Airn* while the other 3 imprinted genes in the cluster are not transcribed. While it is known that *Airn* expression leads to gene silencing, the mechanism remains to be determined¹.

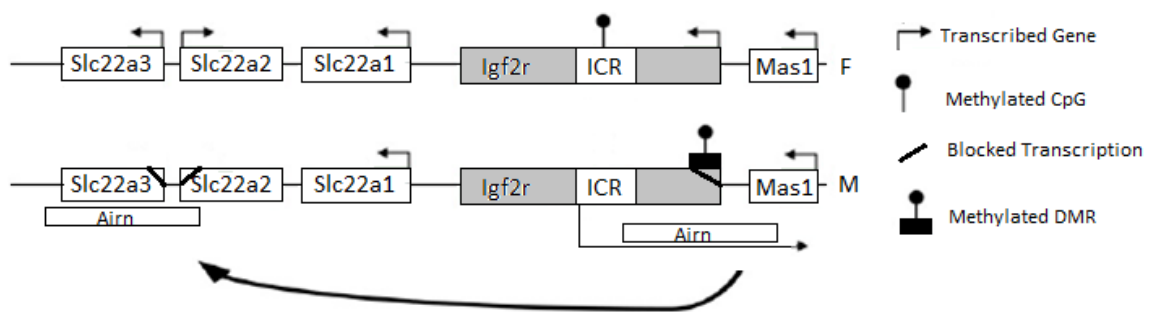


Figure 1.2 Imprinted *Igf2r* cluster. Figure adapted from Bartolomei et al¹.

1.2 X-Linked Imprinting

While most imprinted genes are found on autosomes, a subset has been identified on the X chromosome²⁰. Most X-linked genes, imprinted and non-imprinted, are subject to X chromosome inactivation in female mammals; one X chromosome in each cell is randomly inactivated as a form of dosage compensation to equate for the single (maternal) X chromosome in male cells. A counting mechanism ensures that each cell maintains only one active X chromosome per diploid cell²¹. The inactive X chromosome is a Barr body and is visualized in somatic cells as compact chromatin.

X chromosome inactivation is mediated by the X chromosome inactivation center (XIC) which contains several elements that may play a role in inactivation. One such element is the X-chromosome-controlling element (XCE)²². The X chromosome carrying the stronger XCE is more likely to remain active, leading to unequal X inactivation. Other elements include the genes *XIST* (X (inactive)-specific transcript)²³ and *TSIX* (X (inactive)-specific transcript, antisense)²⁴. *XIST* encodes a 17 Kb noncoding RNA molecule that accumulates along the X chromosome containing the active *XIST* gene, resulting in inactivation of most genes on that chromosome with few exceptions. *TSIX*, also a noncoding transcript, is synthesized on the strand antisense to *XIST* and at the onset of X-inactivation extends along the entire *XIST* gene of the X chromosome destined to remain active. While it is known that *TSIX* regulates *XIST* expression *in cis*, the mechanism by which this occurs is undetermined.

X chromosome inactivation complicates X-linked imprinting by influencing the expression level of X-linked imprinted genes in females. For example, a paternally imprinted gene will be expressed in approximately half of a female's cells. The other half of cells with an inactive maternal X chromosome will have low, if any, expression of the paternally imprinted gene. In comparison, males will express this paternally imprinted gene from their single (maternal) X chromosome in every cell. Consequently, males will exhibit higher expression of this gene than females. The expression difference may contribute to sex-specific differences seen between males and females.

1.3 Search for X-Linked Imprinted Genes

A search for X-linked imprinted genes was performed using a mouse model for Turner syndrome ($39,X^m$ and $39,X^p$)²⁵. The search led to the gene *X-linked lymphocyte regulated (Xlr)*, of which fifteen paralogs have been identified. Of these fifteen, three have been identified as imprinted genes: *Xlr3b*, *Xlr4b* and *Xlr4c* are repressed on the paternal X chromosome²⁵. The *Xlr3* and *Xlr4* gene clusters are in a region of high homology that is highly conserved between mouse and human. In humans, this region is located near the end of Xq28, however no human homologs of any *Xlr* gene have been identified. In addition, the function of *Xlr* proteins remains unclear.

Following identification of the imprinted mouse *Xlr* genes, Dr. Addie May Nesbitt expanded the search for X-linked imprinted genes. Because imprinted genes are typically found in clusters, her search included four genes in a region 1 Mb downstream of the *Xlr* locus and one gene 2Mb upstream: *Filamin alpha* or *Actin binding protein 280/Abp280 (Flna)*, *B cell receptor associated protein 31 (Bcap31)*, *Inhibitor of kappa B kinase gamma (Ikbkg)*, *Transketolase-like 1 (Tktl1)* and *Cd99 antigen-like 2* or *Xap89 (Cd99l2)*. All but one gene displayed biallelic expression in E9.5 embryo, E9.5 placenta and E14.5 liver. The exception was *Tktl1* in liver, where there was a statistically significant difference between the different genotypes. $39,X^m$ *Tktl1* expression was about 14-fold higher than $39,X^p$, while $40,XX$ expression was in between $39,X^m$ and $39,X^p$ with the expression level closer to $39,X^p$. Since X-linked imprinted genes have been implicated in neurocognitive disorders, a variety of brain subregions were assayed as well and analysis found increased *Tktl1* expression in brain subregions of $39,X^m$. Subsequently, *Tktl1* became the focus of X-linked imprinting studies.

Upon confirmation of *Tktl1* imprinting in mice, the search for a human ortholog began. Human brain subregions from a 19 week 40,XX female indicate tissue specific imprinting of *TKTL1*. The hypothalamus, midbrain, frontal cortex and thalamus all displayed higher *TKTL1* expression from one X chromosome while the temporal cortex did not show an imprint. Assays using human lymphoblastoid cells from Turner syndrome individuals demonstrated higher *TKTL1* expression from the maternal X chromosome. Taken together, these results indicate that *Tktl1/TKTL1* is paternally imprinted in both mouse and human.

CHAPTER 2: *TKTL1* Overexpression Studies

2.1 Background Information

Pentose Phosphate Pathway

Glucose metabolism in the cell occurs via two main biochemical pathways: the Embden-Meyerhof pathway and the pentose phosphate pathway (PPP). The Embden-Meyerhof pathway degrades glucose to provide lactic acid and ATP in anaerobic conditions. The PPP exists in the cytoplasm of the cell (Figure 2.1), producing the reducing equivalent NADPH (reduced nicotinamide adenine dinucleotide phosphate) and ribose for ribose nucleic acid. The PPP consists of two branches: the oxidative branch and the nonoxidative branch. The oxidative branch of the PPP is unidirectional, whereas the nonoxidative branch is fully reversible. NADPH is produced in the oxidative branch via the enzymes glucose-6-phosphate dehydrogenase (G6PD) and 6-phosphogluconate dehydrogenase (6PGD). In the nonoxidative branch, the forward reactions produce glyceraldehyde-3-phosphate and fructose-6-phosphate while the reverse reactions produce ribose-5-phosphate.

Transaldolase (TAL) and Transketolase (TK) comprise the enzymes of the PPP's nonoxidative branch. TAL catalyzes two reactions: glyceraldehydes-3-phosphate to fructose-6-phosphate; sedoheptulose-7-phosphate to erythrose-4-phosphate. TK catalyzes the following: xylulose-5-phosphate and ribose-5-phosphate to sedoheptulose-7-phosphate or glyceraldehydes-3-phosphate; xylulose-5-phosphate and erythrose-4-phosphate to glyceraldehydes-3-phosphate or fructose-6-phosphate. Conflicting results have been obtained as to which is the rate-limiting enzyme of this branch^{26,27,28,29}.

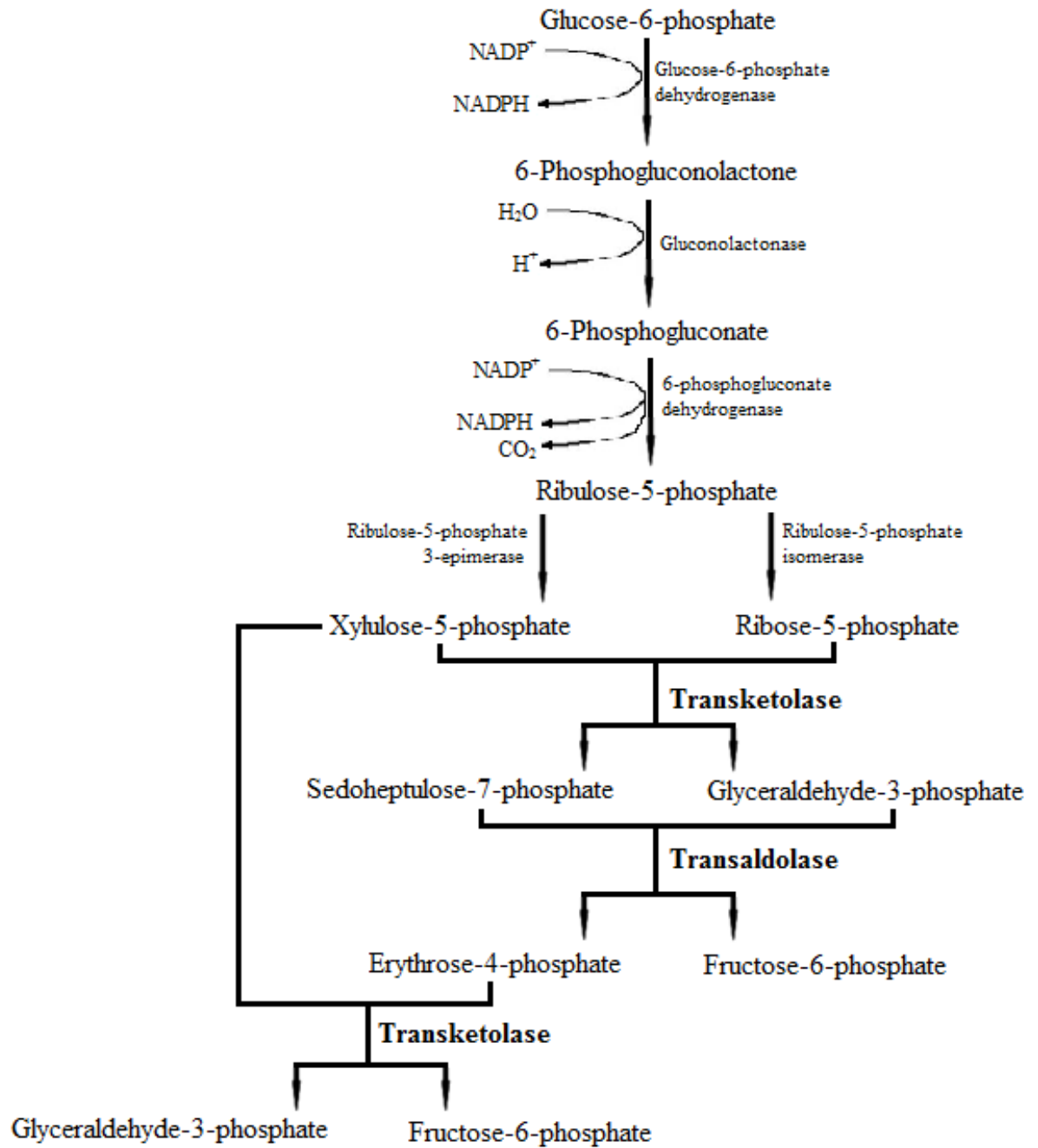


Figure 2.1 The pentose phosphate pathway of glucose metabolism. The oxidative branch begins at glucose-6-phosphate and produces ribulose-5-phosphate, which leads into the nonoxidative branch.

TK transfers a two carbon unit (1,2-dihydroxyethyl) in a two-substrate reversible reaction from ketose phosphates to aldose phosphates. TK is a thiamine-dependent transferase and therefore requires thiamine diphosphate, along with Ca^{2+} , as cofactors^{30,26}. The forward reactions catalyzed by TK produce glyceraldehyde-3-phosphate and fructose-6-phosphate which are utilized by glycolytic pathways or converted into glucose-6-phosphate and reintroduced into the PPP. In the reverse reaction, TK produces ribose-5-phosphate which is necessary for nucleic acid synthesis.

TK has been implicated in neurodegenerative diseases, diabetes and cancer³¹. Thiamine deficiency in humans leads to the neuropsychiatric disorder Wernicke's encephalopathy (WE), which is encountered in chronic alcoholics and patients with impaired nutrition associated with gastrointestinal disease or AIDS³². In Alzheimer's disease, varied TK proteins with different isoelectric points have been detected. Altered TK activity is not implicated in other neurological diseases, making this characteristic for Alzheimer's disease and a potential biomarker³³. Diabetes patients have high blood glucose levels resulting in nonenzymatic glycation which causes vascular complications, neuropathy and retinopathy by producing advanced glycation end products³⁴. Treatment with vitamin B1 (thiamine derivative benfotiamine) supplements activates TK, blocking three major pathways of hyperglycemic damage³⁵. In cancer, some cells produce more than 85% of ribose for nucleic acid synthesis directly or indirectly from the nonoxidative branch of the PPP due to increased enzymatic activity³⁶. Specifically, *transketolase-like 1* upregulation occurs in cancer cells³⁷, providing a novel target for cancer patient nutrition and treatment.

Transketolase-like 1

One transketolase gene, *transketolase (TK)*, and two transketolase-like genes, *transketolase-like 1 (TKTL1)* and *transketolase-like 2 (TKTL2)*, have been identified. *TKTL1*, initially described by Coy et al. in 1996 as a transketolase-related gene, contains a stop codon in a putative exon which causes deletion of that exon. The deletion mutates one of the two thiamine binding sites in the gene. Because of the pseudoexon it was thought that *TKTL1* was a pseudogene, however Coy et al. later demonstrated transketolase activity³¹. *TKTL1* encodes a tissue-specific spliced exon, causing formation of *TKTL1* transcripts which produce full length and smaller proteins and encode tissue-specific protein isoforms. While *TKTL1* acts as a transketolase, it also has altered enzymatic activity. Coy et al. found that *TKTL1* has broader substrate utilization than *TK*, as well as an enhanced one-substrate reaction³¹.

TKTL1 is the sole transketolase upregulated in tumor cells, potentially due to its location; Xq28 is one of a few regions activated in malignancies and during the cell cycle^{39,40}. Cancer cells naturally overexpressing *TKTL1* have an increased amount of reduced glutathione (GSH) and NADPH compared to similar cells in which *TKTL1* has been silenced with siRNA⁴¹. In cancer cells, upregulation of *TKTL1* is thought to increase flow through the oxidative branch of the PPP, leading to increased NADPH production and subsequently increased GSH production. The GSH increase would neutralize free radicals, characteristic of cancer cells, allowing the cancer cell to combat oxidative stress. Silencing *TKTL1*, however, causes the cancer cell to succumb to oxidative stress and apoptose.

2.2 Overexpression Studies

Functional analysis of *TKTL1* overexpression remains to be performed.

Specifically, the effect of *TKTL1* overexpression on oxidative stress has not been studied.

The effect of *TAL* overexpression, however, has been analyzed.

TAL overexpression in Jurkat human T cells leads to decreased enzymatic activities of G6PD and 6PGD and decreased NADPH and GSH levels⁴². Based on these results and others, Banki et al. proposed that *TAL* plays a critical role in regulating the balance between the oxidative and nonoxidative branches of the PPP⁴². I hypothesized that similar results would be obtained upon overexpression of *TKTL1*, coding for the other critical enzyme of the nonoxidative branch of the PPP.

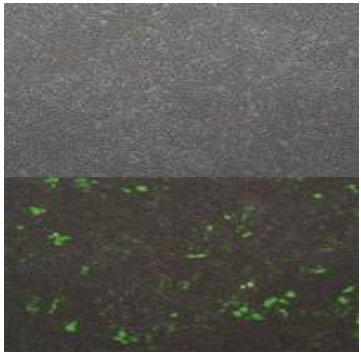
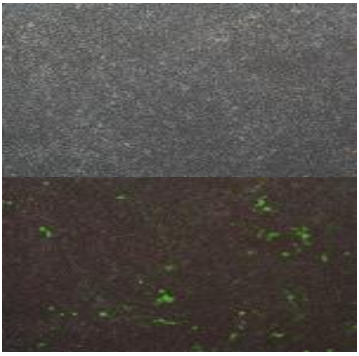




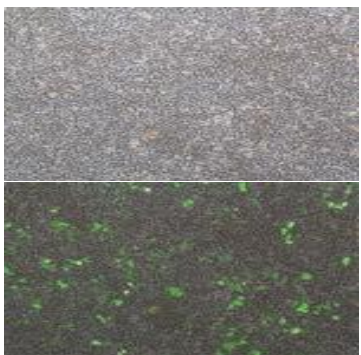
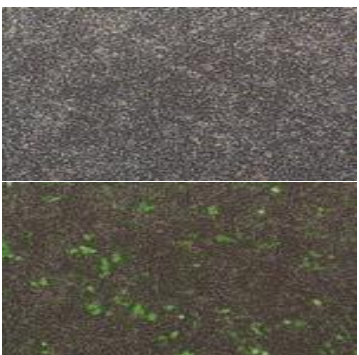
I aimed to determine the effect of *TKTL1* overexpression on oxidative stress. Overall, I hypothesized that *TKTL1* overexpression would lead to increased cellular oxidative stress as measured by the effect of *TKTL1* overexpression on GSH levels. NADPH and *G6pdx* expression levels were also analyzed in effort to determine *TKTL1*'s effect on the PPP. An immortalized mouse hippocampal cell line (HT-22, gift from the laboratory of Dr. Walikonis) was used for transfection. The HT-22 cell line is a glutamate-sensitive subclone from an HT-4 cell line. HT-4 cells were derived from mouse neuronal tissue immortalized with a temperature-sensitive SV40 T-antigen that adopted properties of differentiated neuronal cells at the nonpermissive temperature. *TKTL1* was overexpressed by transfecting HT-22 cells with the human *TKTL1* gene, allowing visualization of the resulting protein by Western blot analysis separately from the mouse protein based on antibody specificity and thus demonstrating *TKTL1* overexpression.

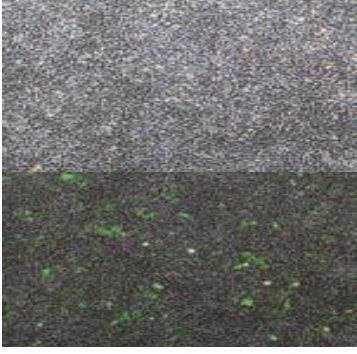
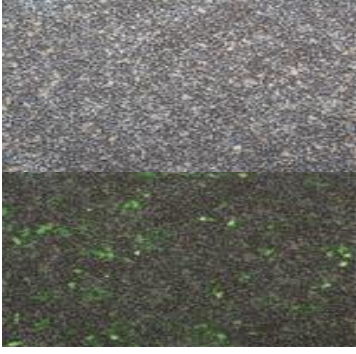
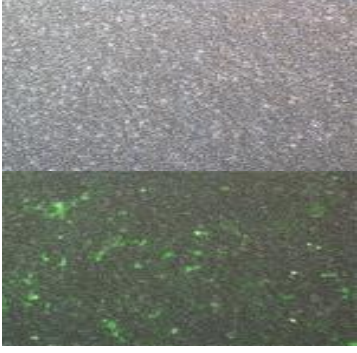
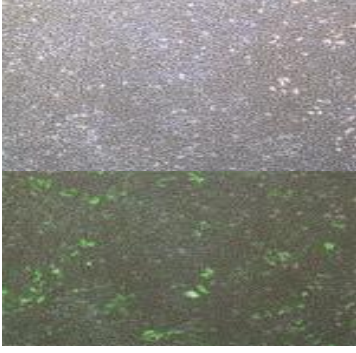
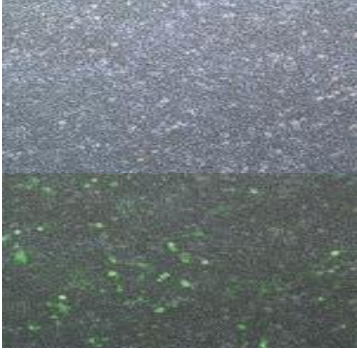

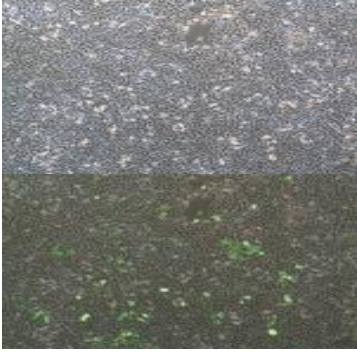
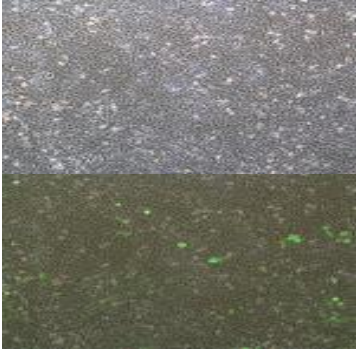
Construct Formation

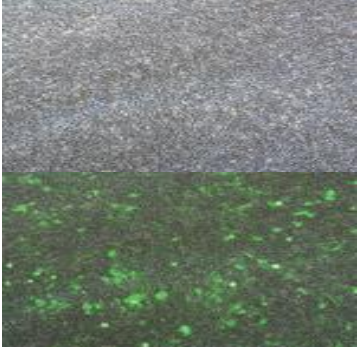
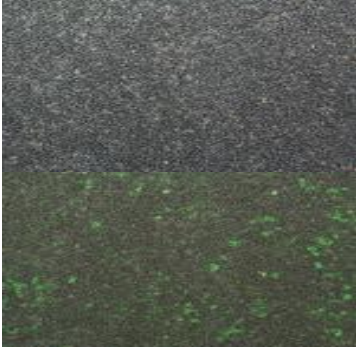
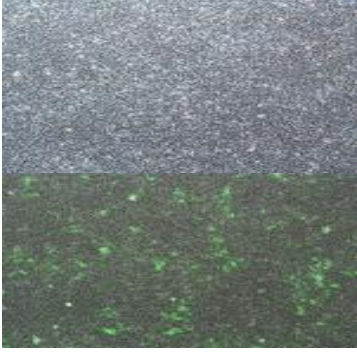
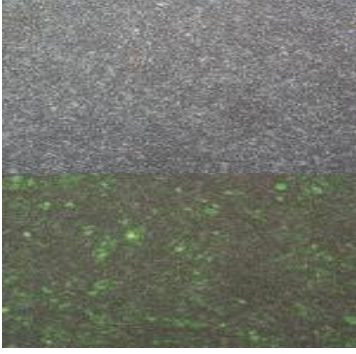
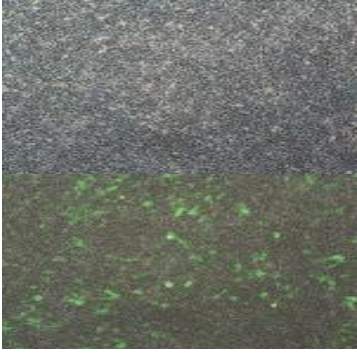
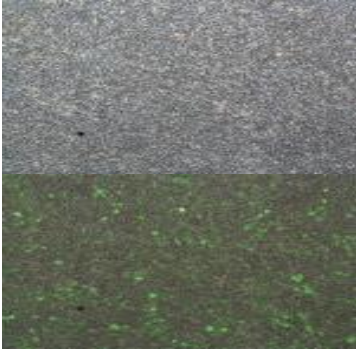
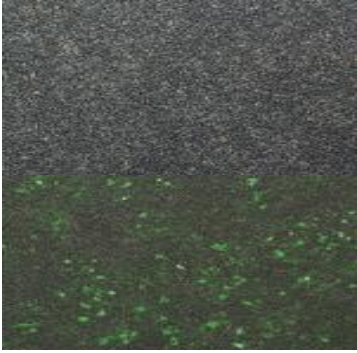
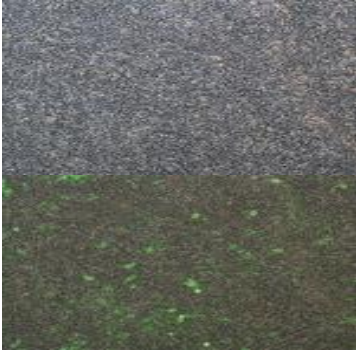
pCAGGS (gift from the laboratory of Dr. LoTurco), a 4801bp plasmid with a constitutive chicken β -actin promoter allowing for constant expression, was used for transfection (Supplemental Figure 1). The human *TKTL1* sequence was inserted into the vector by restriction enzyme digestion and ligation (Protocol 1) and selected for in *Escherichia coli* by the ampicillin resistance cassette on pCAGGS.

Transfection

TKTL1 was overexpressed in HT-22 cells by transfection using Lipofectamine™ LTX (Protocol 2). A GFP-pCAGGS construct (gift from the laboratory of Dr. Walikonis) was co-transfected with the hTktl1-pCAGGS construct in order to visualize transfection efficiency. Green fluorescent protein (GFP) was produced in the cells by the GFP-pCAGGS construct, presumably representing the transfection efficiency of hTktl1-pCAGGS as well. The images in Table 2.1, captured by an inverted microscope, illustrate the GFP expression and the confluency of HT-22 cells on the day they were harvested. There appears to be high transfection efficiency.

Trial	Control	Sample
1	NA	NA
2		
3	NA	NA
4A		
4B		
5A		

5B		
6A	NA	NA
6B	NA	NA
7A		
7B		
7C		

8A	 A rectangular image showing a horizontal split. The top half is a light gray, coarse-grained material, likely gravel or crushed stone. The bottom half is a dark, textured surface with numerous small, bright green spots, possibly representing vegetation or a specific soil type.	 A rectangular image showing a horizontal split. The top half is a dark gray, fine-grained material. The bottom half is a dark, textured surface with numerous small, bright green spots, similar to the image in 8A.
8B	 A rectangular image showing a horizontal split. The top half is a light gray, coarse-grained material. The bottom half is a dark, textured surface with numerous small, bright green spots.	 A rectangular image showing a horizontal split. The top half is a light gray, coarse-grained material. The bottom half is a dark, textured surface with numerous small, bright green spots.
8C	 A rectangular image showing a horizontal split. The top half is a dark gray, fine-grained material. The bottom half is a dark, textured surface with numerous small, bright green spots.	 A rectangular image showing a horizontal split. The top half is a light gray, coarse-grained material. The bottom half is a dark, textured surface with numerous small, bright green spots.
8D	 A rectangular image showing a horizontal split. The top half is a dark gray, fine-grained material. The bottom half is a dark, textured surface with numerous small, bright green spots.	 A rectangular image showing a horizontal split. The top half is a light gray, coarse-grained material. The bottom half is a dark, textured surface with numerous small, bright green spots.

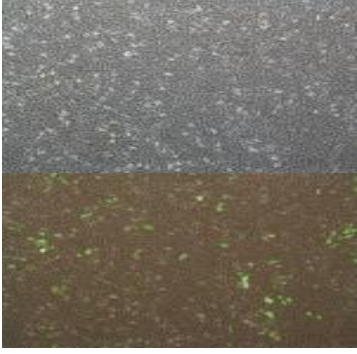

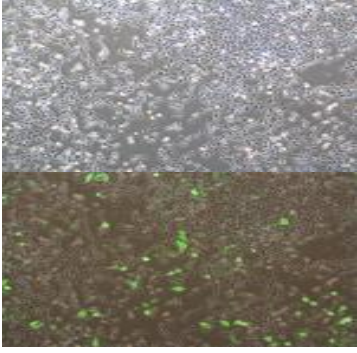


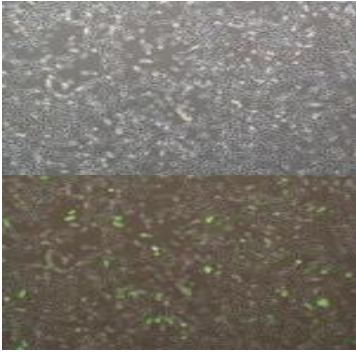






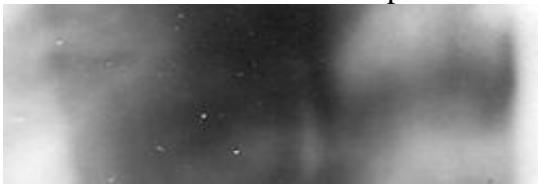
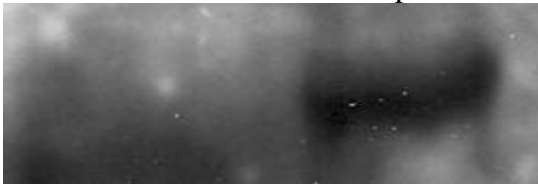
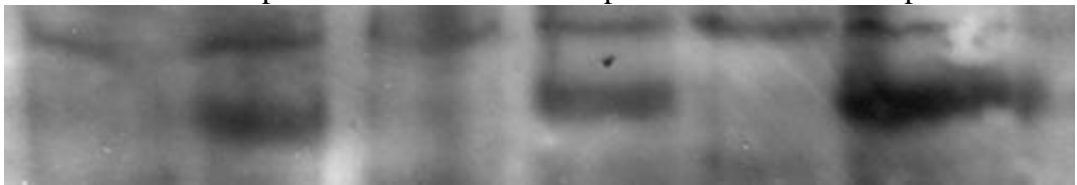

9A		
9B	NA	NA
9C		
9D		

Table 2.1 The first column contains the transfection trial designation. The second column contains images of HT-22 cells transfected with GFP-pCAGGS and pCAGGS (control). In the third column are images of HT-22 cells transfected with GFP-pCAGGS and hTktl1-pCAGGS (sample). Each box contains images of transfected HT-22 cells without visualizing the fluorescence on top and images showing the GFP expression on bottom, thereby indicating the expression of control or hTktl1-pCAGGS. “NA” means that images were not available for the indicated trials.

Western Blot Analysis

After the transfected HT-22 cells were harvested a Western blot was performed to confirm the absence and presence of human TKTL1 in control and sample cells, respectively (Protocol 3). Goat anti-human TKTL1 bound to TKTL1 in hTktl1-pCAGGS transfected cells, but not in control cells, confirming expression of human TKTL1 only in hTktl1-pCAGGS transfected cells (Table 2.2). Therefore, overexpression of *TKTL1* is indicated in cell samples and not controls.

Trial	Western Blot Image	
1	Control	Sample
		
2	NA	
3	Control	Sample
		
4A	Control	Sample
		
4B	Control	Sample
		

5A	<p style="text-align: center;">Control Sample</p> 
5B	<p style="text-align: center;">Control Sample</p> 
6A	<p style="text-align: center;">Control Sample</p> 
6B	<p style="text-align: center;">Control Sample</p> 
7	<p style="text-align: center;">Control A Sample A Control B Sample B Control C Sample C</p> 
8	<p style="text-align: center;">Control A* Sample A Control B Sample B</p>  <p>*Sample A spilled over into the well for Control A upon loading the gel. This control/sample pair was excluded from use in future assays.</p>

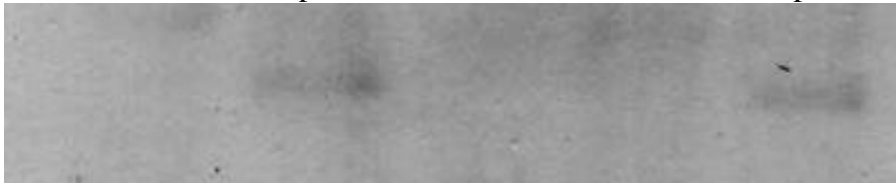

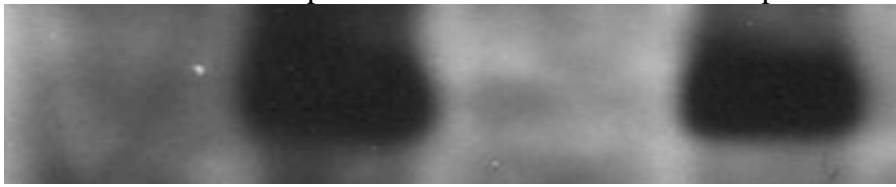
8	<div style="display: flex; justify-content: space-around; text-align: center;"> Control C Sample C Control D Sample D </div> 
9	<div style="display: flex; justify-content: space-around; text-align: center;"> Control A Sample A Control B Sample B </div> 
9	<div style="display: flex; justify-content: space-around; text-align: center;"> Control C Sample C Control D Sample D </div> 

Table 2.2 Detection of the human TKTL1 protein by Western blot in HT-22 cell lines after transfection with GFP-pCAGGS and control (pCAGGS) or hTktl1-pCAGGS (sample). The primary antibody was specific to human TKTL1 and the protein band size is 65kDa. Primary and secondary antibodies bound only to the sample transfected with hTktl1-pCAGGS. A negative control with secondary antibody only was performed with all controls and samples and resulted in a lack of protein bands (data not shown), demonstrating primary antibody specificity.

***TKTL1* Expression Analysis**

Primers were designed that captured both the mouse and human *TKTL1* gene sequence (Supplemental Table 1), made possible by the high sequence homology shared by mouse and human *TKTL1*. Real-time RT-PCR was performed using the designed primers and RNA from control and hTktl1-pCAGGS transfected HT-22 cells (Protocols 4 and 5). The results demonstrate that *TKTL1* gene expression is millions of times greater in hTktl1-pCAGGS transfected cells versus control cells (Figure 2.2); however there is no relation to the amount of TKTL1 protein in the cell samples. Since Western blot

analysis revealed human TKTL1 protein in only the hTktl1-pCAGGS transfected cells, it is reasonable to assume that total TKTL1 protein content is greater in the sample cells than the control cells. Therefore, *TKTL1* is overexpressed in hTktl1-pCAGGS transfected cells compared to control cells.

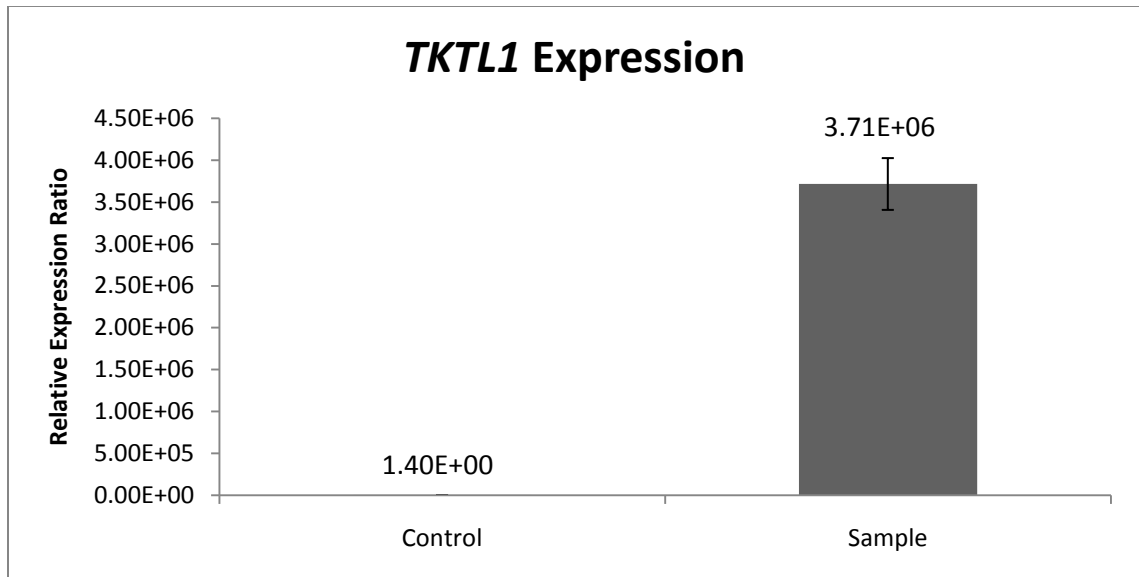


Figure 2.2 Real-time RT-PCR of *TKTL1* in control and hTktl1-pCAGGS transfected HT-22 cells. *TKTL1* transcription level increased by approximately 3 million fold in the hTktl1-pCAGGS transfected cells. The translation level of the gene is not reflected. Error bars indicate a 95% confidence interval.

Glutathione Assay

The Glutathione Assay kit from Cayman Chemical was used to determine the amounts of reduced and oxidized glutathione (GSH and GSSG, respectively) in control and hTktl1-pCAGGS transfected cells (Protocol 6). The kit relies on a colorimetric reaction where GSH reacts with 5,5'-dithio-*bis*-2-(nitrobenzoic acid) (DTNB) to produce 5-thio-2-nitrobenzoic acid (TNB), which has a yellow color. GSHTNB is concomitantly

produced and reduced by glutathione reductase to recycle the GSH and produce more TNB. The rate of TNB production is directly proportional to the GSHTNB to GSH reaction, which is directly proportional to the concentration of total glutathione. The absorbance of the yellow TNB at 405nm provides an estimation of total glutathione in a sample. In order to determine GSH amount alone, GSSG can be measured and subtracted from the total glutathione. Measurement of GSSG is performed similarly to total glutathione measurement, but with the addition of 2-vinylpyridine to the sample to derivatize glutathione. GSH and GSSG concentrations were calculated using the end point analysis method. Statistical methods were also used to analyze the data.

Glutathione Assay Results

Nine different HT-22 cell lines were assayed for GSH and GSSG, four of which resulted in negative amounts of GSSG in control and/or hTktl1-pCAGGS transfected cells. In other words, the absorbance values were less than the 0mM GSSG standard absorbance potentially due to negligible amounts of GSSG, insufficient cell concentration, or interference as suggested through communications with Cayman Chemical technical support. The cell samples were concentrated as much as possible and in some cases resulted in positive amounts of GSSG, while others remained negative.

Figure 2.3 displays the GSH/GSSG redox ratio for the five trials that resulted in positive concentrations. The ratio for trials 3, 6 and 8 decreased upon overexpression of *TKTL1*, while Trials 7 and 9 showed no difference. The GSH/GSSG ratios and standard deviations can be found in the supplemental information (Table 2).

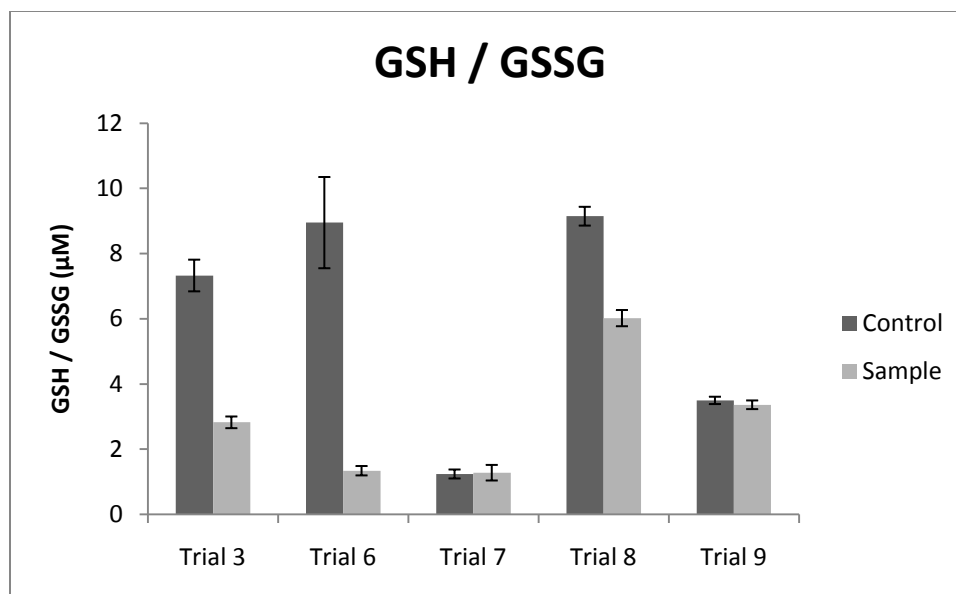


Figure 2.3 GSH/GSSG in control and hTkt11-pCAGGS transfected HT-22 cells. These were the trials that resulted in positive concentration values. *TKTL1* overexpression resulted in decreased GSH/GSSG ratios or no difference. Error bars indicate a 95% confidence interval.

The raw absorbance values obtained for all nine glutathione assays were also analyzed. Initially, the proportion of GSH in each cell sample was calculated (Table 2.3 and Figure 2.4) using the formula $(GSH - GSSG) / GSH$. Since GSH in the assay represents total glutathione, the absorbance value for oxidized glutathione was subtracted from the GSH value to give the value for reduced GSH.

GSH / Total Glutathione

Trial #	Control	Sample
1	0.21173	0.15589
2	0.71477	0.59042
3	0.57010	0.43391
4	0.75465	0.74759
5	0.78521	0.71819
6	0.47580	0.11955
7	0.11657	0.12729
8	0.60528	0.55941
9	0.38604	0.40499

Table 2.3 Proportion of GSH in control and hTktl1-pCAGGS transfected cells.

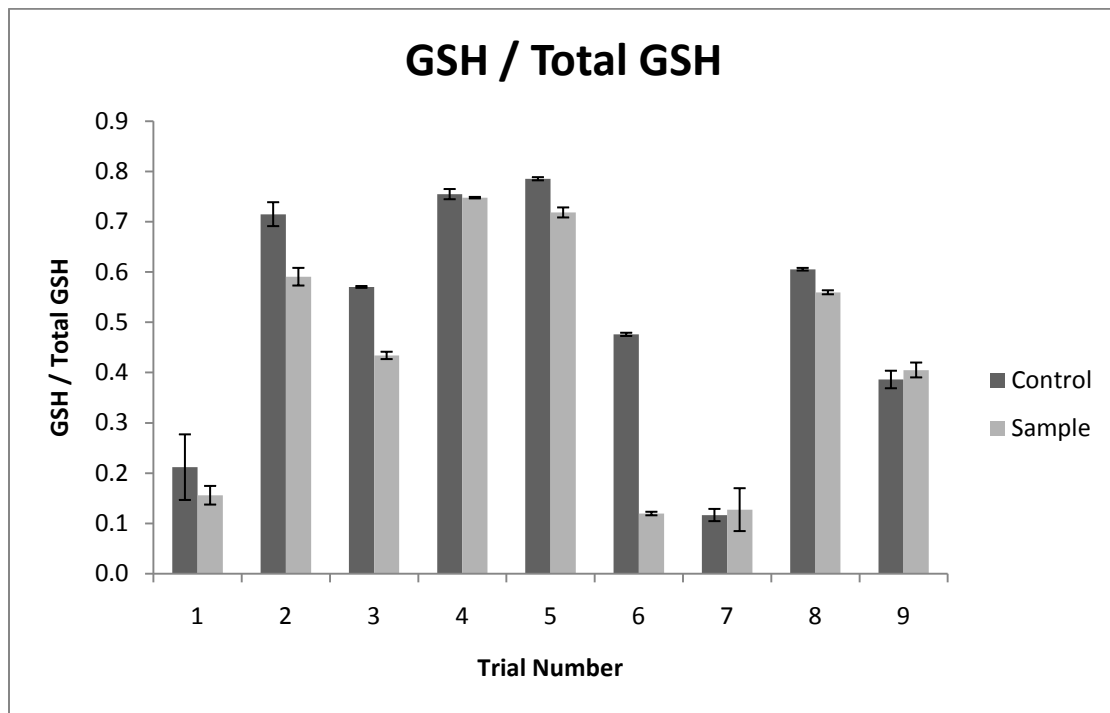


Figure 2.4 Proportion of GSH in control and hTktl1-pCAGGS transfected cells for all nine trials. Five trials resulted in a decreased proportion upon *TKTL1* overexpression, four trials displayed no change. Error bars indicate a 95% confidence interval.

A boxplot was then constructed to visualize the data (Figure 2.5). The boxplot illustrates that the proportion of GSH in HT-22 cells decreased upon *TKTL1* overexpression. The decrease is statistically significant ($P = 0.029$) as determined by a one-tailed T-test.

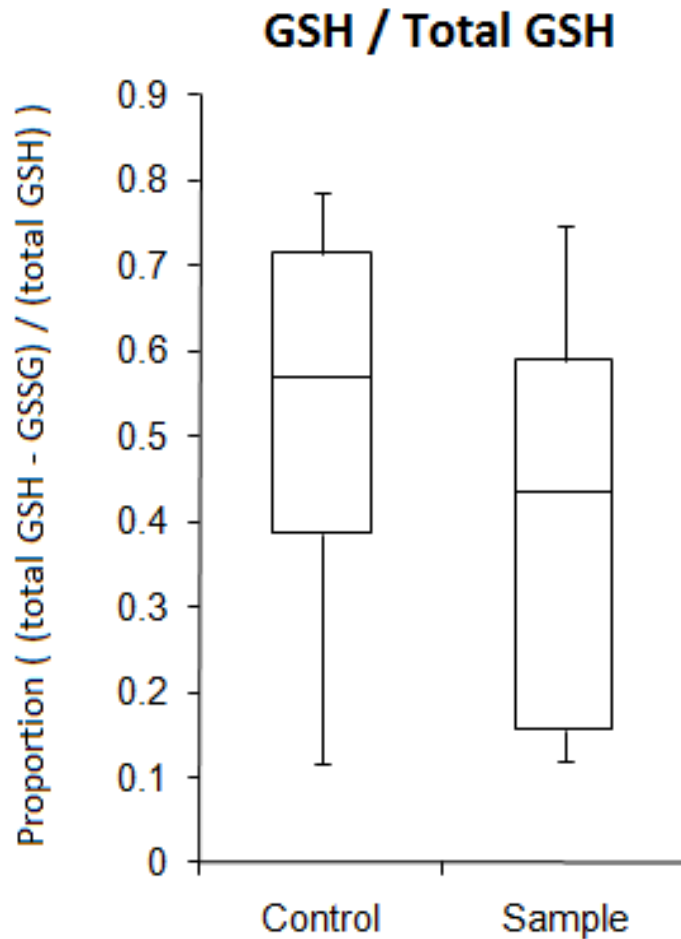


Figure 2.5 Boxplot of the proportion of GSH in control and hTktl1-pCAGGS transfected HT-22 cells using raw absorbance values ($P = 0.029$).

Glutathione Assay Analysis

Taken together, the analysis of the concentrations of GSH and GSSG in control and hTktl1-pCAGGS transfected cells and the analysis of the proportion of GSH in the cells based on raw absorbance values indicate that *TKTL1* overexpression decreases the amount of GSH in the cell. Presumably, the cell would not be able to readily reduce free radicals, causing a state of oxidative stress. Based on the PPP, TKTL1 indirectly affects glutathione through influencing NADPH production. I hypothesized that NADPH will also be decreased, providing a mechanism which hinders GSH production.

NADPH Experiments

The NADP⁺/NADPH Assay kit from BioAssay was used to determine the ratio of NADPH/NADP⁺ in the control and hTktl1-pCAGGS transfected cells (Protocol 7). The kit has a procedure to extract NADP⁺ and NADPH from the cells using provided buffers. NADP⁺ and NADPH are then measured by a colorimetric reaction where formed NADPH reduces a formazan (MTT) reagent, which produces a color that is measured at 565nm. This color is proportionate to the NADP⁺/NADPH concentration in the sample.

NADPH Assay Results

Five different HT-22 cell lines were assayed for NADP⁺ and NADPH. Of the five, three displayed a decrease in the NADPH/NADP⁺ ratio upon *TKTL1* overexpression, one increased and one resulted in no change (Figure 2.6). The NADPH and NADP⁺ concentrations and their ratio can be found in Supplemental Table 3.

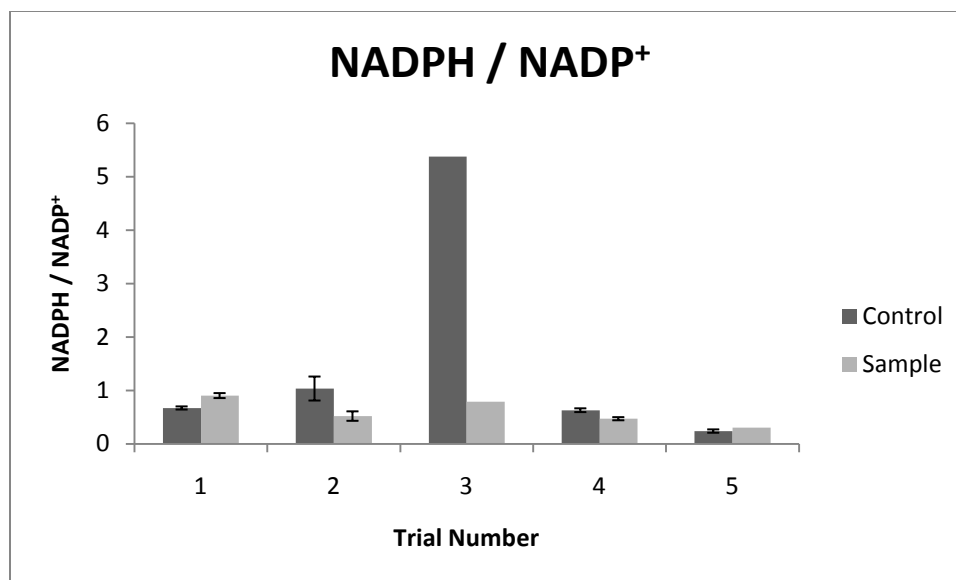


Figure 2.6 NADPH/NADP⁺ ratio for trials 1 through 5. *TKTL1* overexpression resulted in decrease, increase, or no change. Error bars indicate a 95% confidence interval.

NADPH Assay Analysis

Further analysis of NADPH/NADP⁺ is needed in order to provide a conclusive statement about the effect of *TKTL1* overexpression on the NADPH/NADP⁺ ratio. The results suggest that there is an effect on the NADPH/NADP⁺ ratio since the ratio decreased in three out of five trials when *TKTL1* was overexpressed. Since GSH was demonstrated to decrease, it was expected that NADPH would provide the same result. The hypothesized mechanism was that a decrease in NADPH would lead to a decrease in GSH, since NADPH reduces GSSG.

A decrease in the NADPH/NADP⁺ ratio would indicate that overexpression of *TKTL1* decreases the amount of NADPH produced by the cell. Since increase, decrease and no change were all seen, it is possible that NADPH from other sources in the cell is skewing the result. A different assay may be needed to determine the effect of *TKTL1*

overexpression on NADPH/NADP⁺, if any. Based on the Banki et al. paper, it is expected that NADPH will be affected.

***G6pdx* Expression**

Real-time RT-PCR was performed to analyze *G6pdx* expression in control and hTktl1-pCAGGS transfected cells (Protocol 5). Analysis demonstrated a significant decrease of *G6pdx* when *TKTL1* was overexpressed (Figure 2.7).

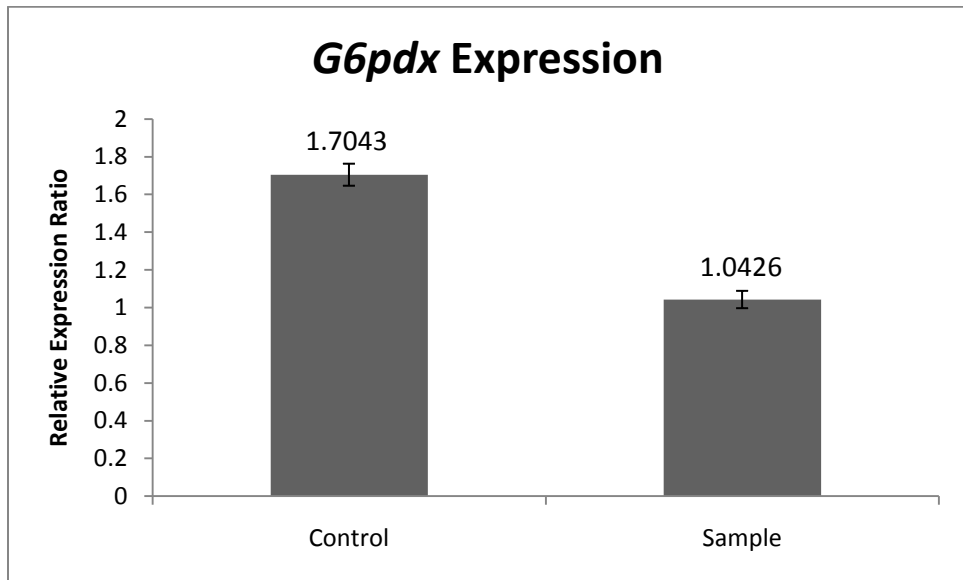


Figure 2.7 Real-time RT-PCR of *G6pdx*, coding for G6PD in mouse, in control and hTktl1-pCAGGS transfected HT-22 cells. *G6pdx* levels significantly decreased upon *TKTL1* overexpression ($P = 0.000135$). Error bars indicate a 95% confidence interval.

***G6pdx* Expression Analysis**

A decrease in *G6pdx* may lead to a decrease in NADPH production since *G6pdx* catalyzes the production of NADPH. Furthermore, less NADPH would be available in the cell to reduce GSSG to GSH, causing a decrease in GSH in the cell and leading to oxidative stress.

Discussion

G6pdx expression decreased due to overexpression of *TKTL1*. It was thought that this decrease would reduce the amount of NADPH produced in the cell. While the results point toward this effect, no conclusion can be made about the actual effect, if any, on NADPH. Assuming there were less NADPH available, the ability of the cell to reduce glutathione would be inhibited. The results demonstrate that the amount of GSH in the cell decreased in response to *TKTL1* overexpression. Based on this result, I determine that the cell is in a state of oxidative stress due to overexpression of *TKTL1*. To confirm this, direct analysis of reactive oxygen species (ROS) levels would be necessary. Increased ROS levels are expected based upon the results of this study and would support the conclusion of oxidative stress. The increase in ROS levels would also increase the cell's sensitivity to apoptosis, which is measurable as well. This was the result upon *TAL* overexpression⁴² and I hypothesize the same effect for *TKTL1* overexpression. Therefore, future analysis may conclude that *TKTL1* levels in the cell play a role in programmed cell death.

ROS, including superoxide, hydroxyl, hydrogen peroxide, singlet oxygen and nitric oxide, cause cellular damage and maintain importance in autism⁴³. Increased ROS levels have been found in patients with autism, as well as in other neuropsychiatric conditions⁴⁴. Impairment in the cell's antioxidant defense system may contribute to this increase. Patients with autism have a decreased amount of reduced GSH compared to unaffected individuals⁴⁵ which decreases the cell's capacity to reduce ROS and leads to oxidative stress. It is unclear, however, if oxidative stress contributes to the pathogenesis of autism, or if it is a secondary manifestation of the disorder⁴⁵.

Chapter 3: Human Lymphoblast Autism Studies

3.1 Background Information

Autism

Autism is a neurodevelopmental syndrome with genetic and nongenetic causes, characterized by a variety of phenotypes. According to the Diagnostic and Statistical Manual of Mental Disorders: DSM-IV-TR there are three criteria for diagnosing autism: impairment in 1) social interaction and 2) communication and 3) restricted patterns of behavior, interests and activities. If a patient has severe impairment in several criteria but not all, the DSM-IV-TR identifies the disorder as pervasive developmental disorder, or autism spectrum disorder (ASD) including autistic disorder, Rett's Disorder, childhood disintegrative disorder, Asperger's disorder, and pervasive developmental disorder not otherwise specified.

Nongenetic factors, such as oxidative stress, contribute to the pathogenesis of autism and several other neuropsychiatric disorders due to the brain's vulnerability to oxidative stress⁴⁶. Research shows lowered levels of the antioxidant enzymes glutathione peroxidase and superoxide dismutase in autistic individuals, denoting impaired antioxidant defense mechanisms⁴⁷. Additionally, patients with autism displayed reduced levels of total glutathione and a lowered GSH/GSSG redox ratio⁴⁸. Supplementation with methyl B12 improved blood glutathione levels and the GSH/GSSG redox ratio in 30% of test subjects, indicating methyl B12 as a potential beneficial autism treatment⁴⁹. Genetic and environmental effects may increase vulnerability to oxidative stress in autism.

Inconsistent linkage and association results⁵⁰, as well as low sibling recurrence compared to single-gene diseases⁵¹, support the genetic complexity of autism. Multiple genetic loci on several chromosomes have been linked to autism or ASD⁵². While some genes are directly linked to autism, others are thought to contribute indirectly by increasing an individual's susceptibility to the disorder. The complex inheritance patterns formed by the combination of multiple genes that interact with each other and the environment remain unknown. Recently, de novo copy number variation mutations have been associated with a subset of ASD cases, typically of individuals with older fathers, leading researchers toward a new mode of inheritance⁵³. One example is the chromosomal region 15q11-q13⁵⁴. This region is an original region associated with autism and is also imprinted in Angelman and Prader-Willi syndromes (AS and PWS, respectively)⁵⁵. An imprint mutation causes either AS or PWS depending on parental mode of inheritance.

Several disorders are consistently associated with ASD, such as fragile X, Angelman and Prader-Willi syndromes, among others, however these cases account for only a small percentage of ASD diagnoses. Notably, all ASD-related syndromes are limited to the brain⁵⁶.

Genome-wide association studies (GWAS) are becoming increasingly important in the study of autism. GWAS have demonstrated that not only is rare variation important in autism, but common variation is as well. GWAS have identified regions and single nucleotide polymorphisms linked or associated with autism. The chromosomal region 15p14.1 is an example of a common variation region⁵⁷. Two genes previously connected to ASD, *RyR2* and *UPP2*, were also identified by GWAS as autism-associated genes⁵⁸.

Autism is diagnosed four times as often in males as in females indicating involvement of an X-linked imprinted gene in autism⁵⁹. Turner syndrome studies by Skuse et al. point toward an X-linked gene that is paternally expressed⁶⁰.

Turner Syndrome and Skuse Hypothesis

Turner syndrome is characterized by complete or partial absence of one X chromosome in some or all of a female's cell lines due to failed sex chromosome segregation. Turner individuals tend to have clinical problems, such as cardiovascular and kidney problems, and exhibit social behavior problems; however their intelligence is typically normal. Skuse et al. found that differences in social behavior could distinguish 45,X^p females from 45,X^m females⁶⁰. The study showed that 46,XX and 45,X^p females had superior social cognitive skills than 46,X^mY males and 45,X^m females indicating that a gene expressed only from the paternal X chromosome is involved in social behavior⁶⁰. If an X-linked imprinted locus is responsible for social behavior differences this may explain why males tend to be affected more often than females by pervasive developmental disorders affecting social behavior, such as autism.

Researchers proposed that a maternal imprint on the X chromosome lowers the threshold for phenotypic expression of the genes predisposing an individual to autism⁶¹. Particularly, this explains the male vulnerability to autism. Looking at this proposal another way, the imprint protects females from developing the disorder.

Another theory is the Baron-Cohen fetal testosterone exposure theory⁶². Baron-Cohen proposed that fetal exposure to high androgen levels is associated with increased severity of some autistic traits, irrespective of sex chromosome constitution. He called

this the “extreme male brain.” The male brain type is defined as one that is superior in understanding physical objects over social common-sense; a female brain type is opposite of this. Individuals are assumed to fall within a continuum in regard to male and female brain types. Furthermore, an individual may be “cognitively balanced” where they show equal male and female brain types. Baron-Cohen suggested that autistic individuals have an extreme male brain type, regardless of sex. Depending on how extreme the male brain type is, an individual would fall on a continuum ranging from a touch of autism to classical autism. It remains controversial as to the neurobiological composition of a male versus female brain.

3.2 Human Lymphoblast Studies

As described previously, oxidative stress has been implicated in the pathogenesis of autism. My study indicates that *TKTL1* overexpression increases oxidative stress, providing a potential connection to autism. Consequently, I aimed to determine if there is a higher level of *TKTL1* expression in relation to autism.

Family studies were executed for comparison of *TKTL1* expression levels in autistic individuals versus their unaffected siblings. Human lymphoblastoid cell lines were obtained from Rutgers University Cell and DNA Repository. The cell lines belonged to individuals affected with autism or ASD (as diagnosed by the DSM-IV) and their unaffected siblings.

***TKTL1* Expression Results**

The lymphoblastoid cell lines of siblings from six pedigrees were brought up in cell culture according to procedures provided by Rutgers University Cell and DNA Repository (Protocol 8). Total RNA was extracted from the obtained lymphoblastoid cell pellets and was analyzed for *TKTL1* expression by real-time RT-PCR (Protocol 9). All real-time RT-PCR results are located in Supplemental Figures 2 through 8. The real-time RT-PCRs were repeated one or more times from the same total RNA.

The graphs in Figures 3.1 through 3.4 represent the autistic and unaffected males from the pedigrees that contained both types of males. We were more interested in comparing males to each other because of skewed X-inactivation patterns in female lymphoblastoid cell lines. Female lymphoblastoid cell lines tend to be mostly XiX or XXi, whereas male lymphoblastoid cell lines will always have an active maternal X chromosome. Since *TKTL1* is imprinted on the paternal X-chromosome, X-inactivation patterns in the cultured female lymphoblasts may therefore skew the *TKTL1* expression results.

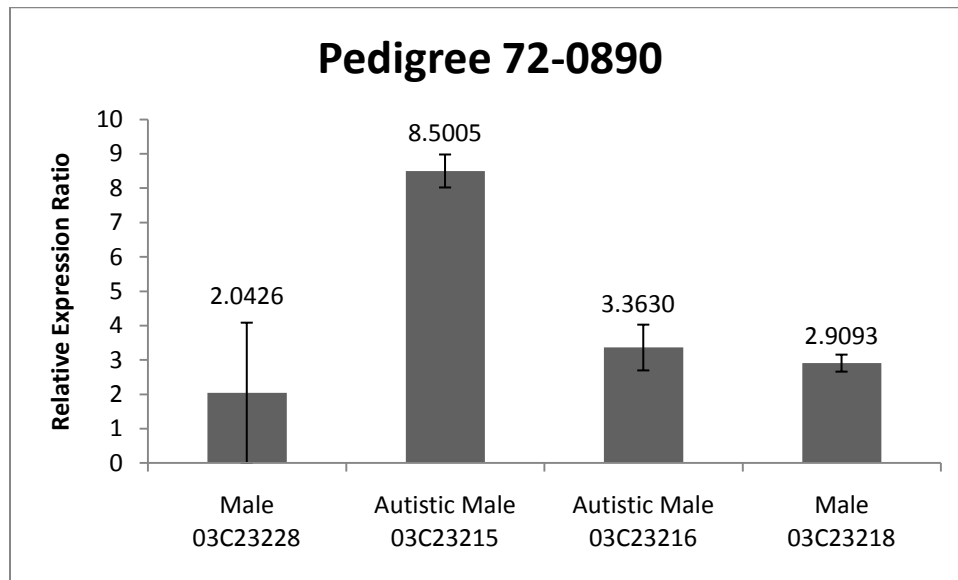
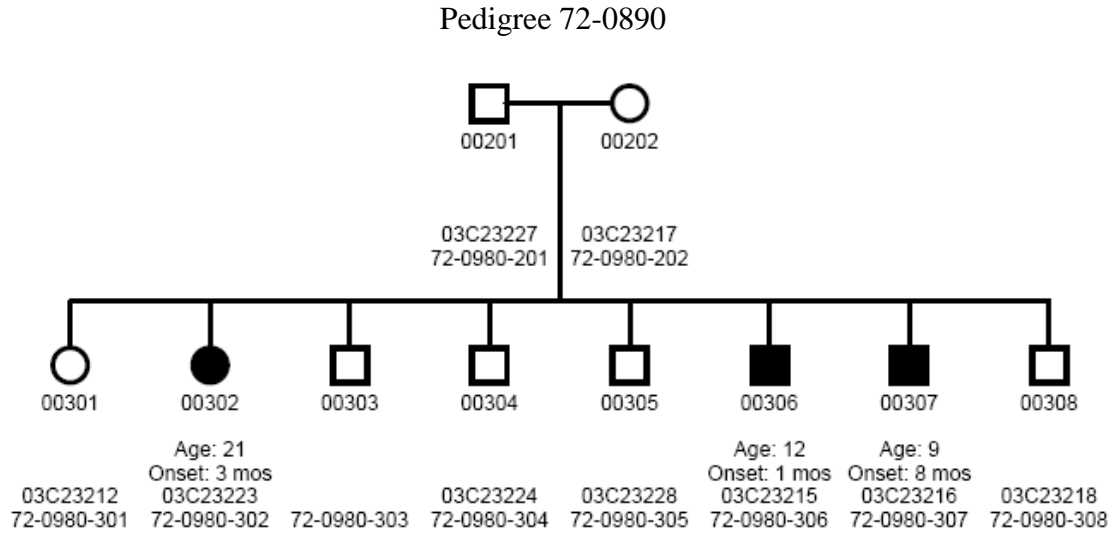


Figure 3.1 Real-time RT-PCR results for *TKTL1* expression in autistic and unaffected males for pedigree 72-0890. Error bars indicate a 95% confidence interval.

Pedigree 72-0890 displayed autistic male 03C23215 as having the highest *TKTL1* expression level. Following, autistic male 03C23216 and unaffected male 03C23218 had similar expression levels to each other. Unaffected male 03C23228 displayed the lowest *TKTL1* expression; however the 95% confidence interval was very large.

Pedigree 74-0264

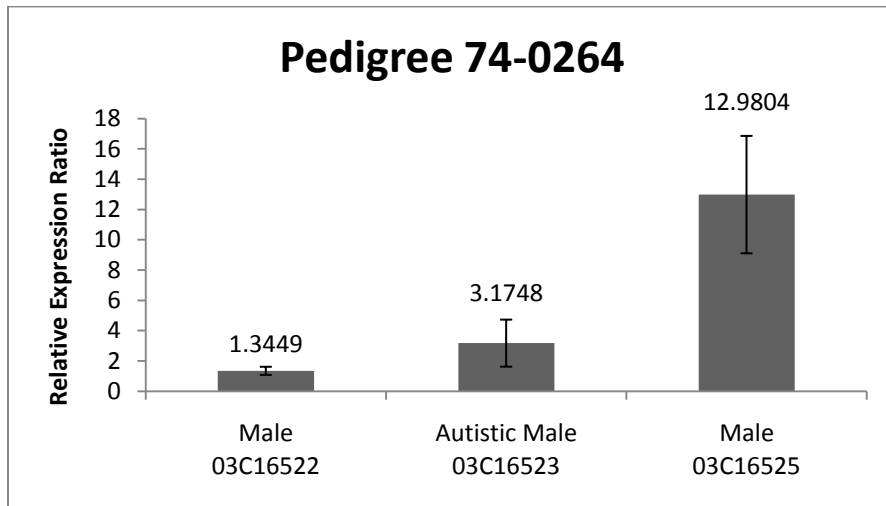
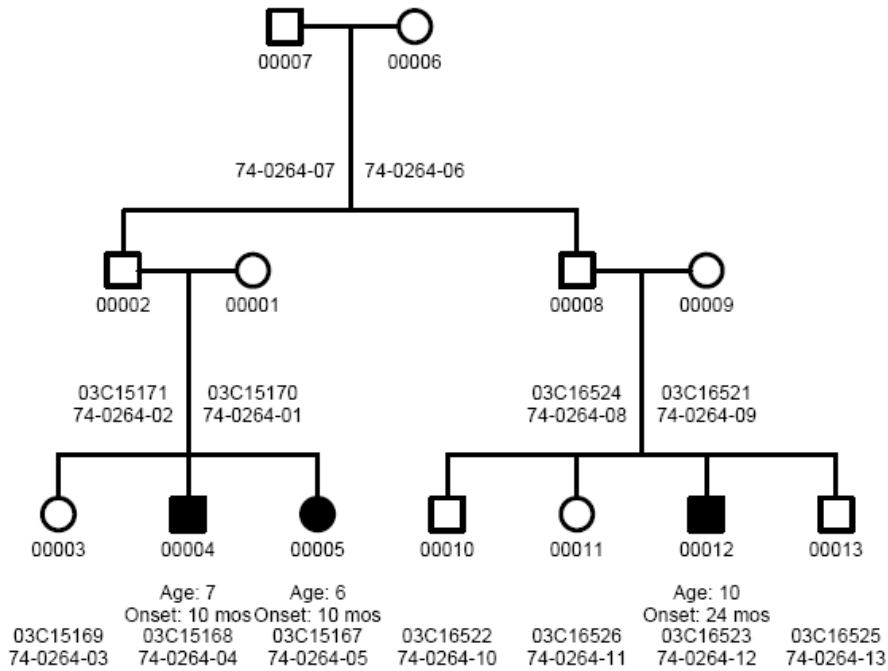


Figure 3.2 Real-time RT-PCR results for *TKTL1* expression in autistic and unaffected males for pedigree 74-0264. Error bars indicate a 95% confidence interval.

Unaffected male 03C16525 displayed the highest *TKTL1* expression level in pedigree 74-0264. The other unaffected male, 03C16522, had the lowest expression, while autistic male 03C16523 displayed an expression level in between the unaffected males, though closer to 03C16522.

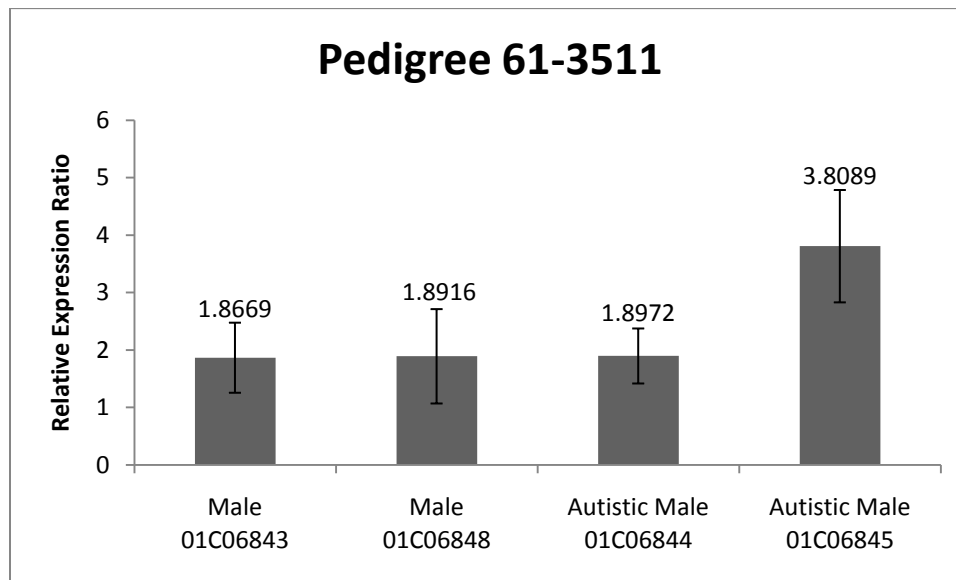
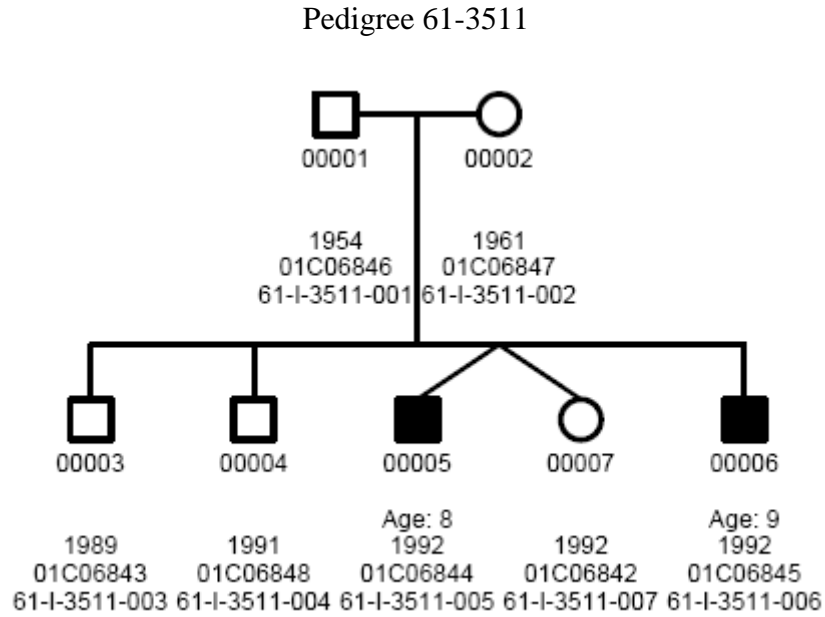


Figure 3.3 Real-time RT-PCR results for *TKTL1* expression in autistic and unaffected males for pedigree 61-3511. Error bars indicate a 95% confidence interval.

An autistic male (01C06845) again displayed the highest expression of *TKTL1* in pedigree 63-3511. The other autistic male (01C06844) and the unaffected males (01C06843 and 01C06845) had expression levels similar to each other but lower than autistic male 01C06848.

Pedigree 63-156

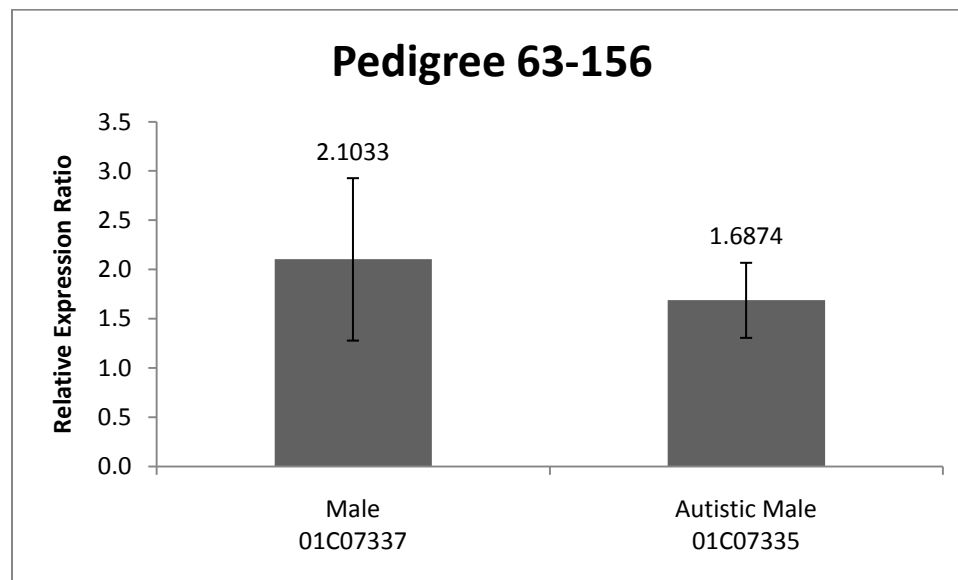
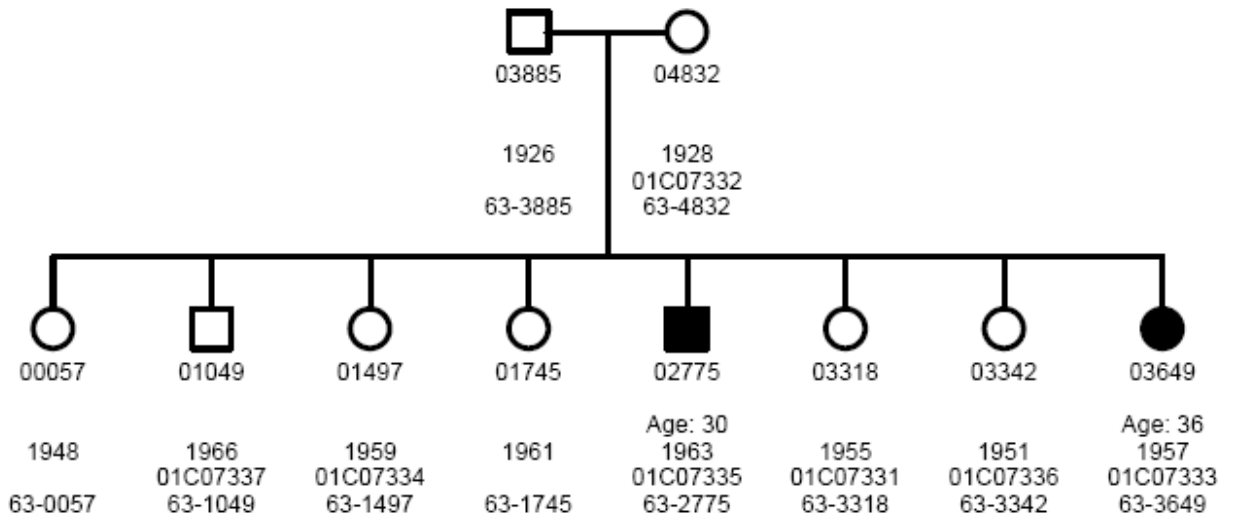


Figure 3.4 Real-time RT-PCR results for *TKTL1* expression in autistic and unaffected males for pedigree 63-156. Error bars indicate a 95% confidence interval.

Finally, pedigree 63-156 contained one unaffected male and one autistic male. They appear to similarly express *TKTL1*; however there may be a chance that male 01C07337 expresses *TKTL1* at a higher level than autistic male 01C07335. The large error bars make this relationship difficult to determine.

***TKTL1* Expression Analysis**

It appears that autistic males may have approximately equal or higher *TKTL1* expression than unaffected male siblings, with one exception. Autistic male 03C16523 in pedigree 74-0264 had lower expression than one of his unaffected brothers (03C16523).

The results for the males analyzed in the above four pedigrees were analyzed together and combined into autistic and control (unaffected) groups. Figure 3.5 displays the individuals' *TKTL1* expression levels along with their averaged expression. The two groups appear to have similar *TKTL1* expression according to this analysis, with a fairly similar distribution of individual expression. A one-tailed T-test determined that there was no significant difference of *TKTL1* expression between autistic and unaffected groups ($P = 0.41417$).

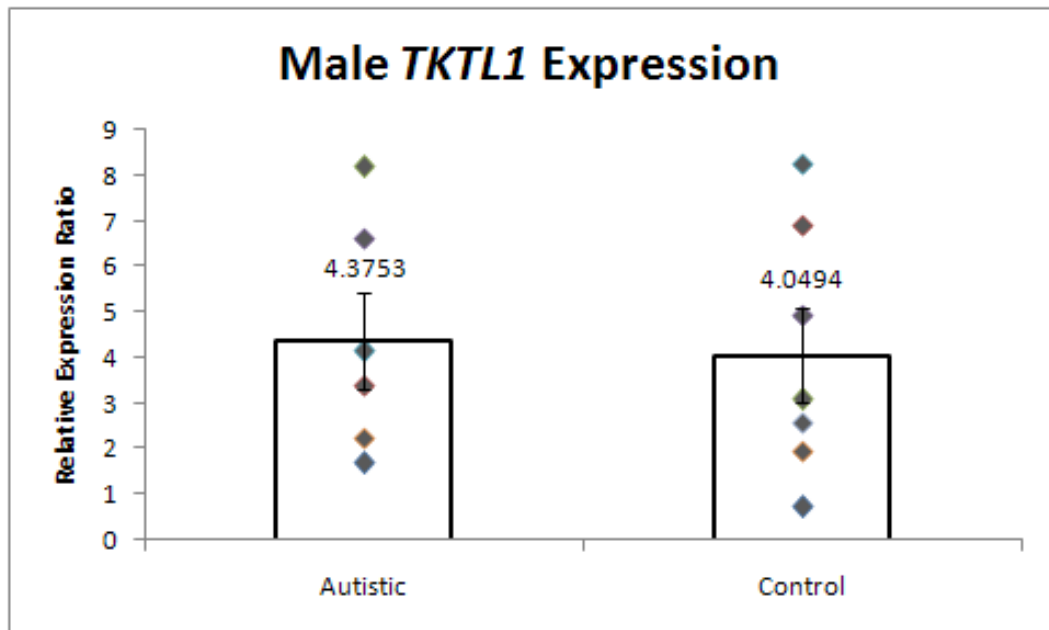


Figure 3.5 *TKTL1* expression in autistic and control (unaffected) males from pedigrees 72-0890, 74-0264, 61-3511 and 63-156. Diamonds indicate individual expression levels for each male. Error bars indicate standard error.

An analysis of variance (ANOVA) was performed by Dr. Nathaniel Jue to further analyze the data. The results of the ANOVA are provided in Tables 3.1 and 3.2. The test indicates that there is no significant difference of *TKTL1* expression between autistic and unaffected individuals. Additionally, both autism (fixed factor) and family (random factor) have no significant effect on *TKTL1* expression.

Source	DF	Sum of Squares	Mean Square	F Ratio
Model	4	16.888646	4.22216	0.7623
Error	8	44.309982	5.53875	Prob > F
C. Total	12	77.814871		0.5782

Table 3.1 Analysis of Variance.

Source	Nparm	DF	DFDen	Sum of Squares	F Ratio	Prob > F
Autistic	1	1	8	0.20472	0.0368	0.8526
FamilyID & Random	4	3	8	16.545622	0.9957	0.4428

Table 3.2 Effects Tests.

Discussion

The information in Figure 3.5 and Tables 3.1 and 3.2 suggests that *TKTL1* expression differences do not exist between autistic and unaffected individuals. However, it must be taken into account that the sample size is relatively small. In total, thirteen males from four families were included in the above figure, which may not be representative of the larger population. The potential differences in *TKTL1* expression that are implicated in Figures 3.1 through 3.4 may also be misleading because of two

problems: real-time RT-PCR C_t values varied within triplicates for an individual and relative expression ratios varied for an individual between trials.

Observation of the C_t values for both *GAPDH* and *TKTL1* revealed variation within the triplicates for a single individual. Variation could be attributed to poor primer design or old primers that degraded. Originally, polyA selected mRNA had been used for real-time RT-PCR, along with a different *TKTL1* primer set. *TKTL1* was difficult to amplify with these primers and produced poor melt curves. I discovered that the forward primer of that set had been designed to pick up a wild type SNP in the 5' UTR of *TKTL1*. With this knowledge, I decided that this was an unacceptable primer set to use and instead made a primer set spanning exons 4 and 5 of the gene. The new primer set amplified *TKTL1* well from total RNA and the polyA mRNA selection was abandoned. For a period of time the C_t values had little variation within the triplicates, however within two months the C_t values started to vary. Since the *GAPDH* C_t values had not previously varied, I ordered the same primers again. Even with fresh primers the C_t values continued to vary within triplicates. Re-ordering the same *GAPDH* primers demonstrated that the variation was probably not due to degraded primers seeing as the issue persisted. It is also interesting to note that both sets of primers had previously amplified the genes well and consistently.

The variation of C_t values within the triplicates for a single individual and the occurrence of this happening for both primer sets caused two problems with the real-time RT-PCR results. First, many error bars on the graphs are very large, meaning that the 95% confidence intervals are very large. Repeating the real-time RT-PCRs did not fix this, however repetition caused the second problem to become apparent. Between trials

the relative expression of *TKTL1* among individuals changed even though the same RNA was used. For example, in pedigree 61-3511 on 3/30/11 autistic male 01C06844 displayed higher *TKTL1* expression than male 01C06848; however that relationship switched on 3/31/11 (Supplemental Figure 2.6). For this reason I took into account the data from all repetitions of pedigrees 61-3511 and 63-156 for the above analysis of unaffected males versus autistic males, however in actuality the relationships may be different. The data from only one trial each of pedigrees 72-0890 and 74-0264 was used for the above analysis because even larger error bars would have been introduced if more data was included. Again, the relationship between individuals may not be accurately represented.

While *GAPDH* has been used as a reference gene in many publications, 18S rRNA is less variable in expression level than *GAPDH* and therefore may be a better candidate for a reference gene. *GAPDH* mRNA levels are not constant⁶³ and expression level variability was found in Epstein-Barr virus-transformed lymphoblastoid cell lines⁶⁴. Another possibility is that both primer sets were poorly designed and for an unknown reason were able to consistently amplify for some triplicates in earlier real-time RT-PCRs. Primer instability and degradation are also concerns. Fresh primer dilutions were made for each real-time RT-PCR, introducing freeze-thaw effects. Masters mixes were used whenever possible to prevent sample-to-sample and well-to-well variability; however automation of the sample preparation would reduce inconsistencies. It is also possible that the RNA degraded over time, possibly due to freeze-thawing the RNA on multiple occasions, or possible nuclease contamination. Variability could also be caused by lot-to-lot inconsistencies of reverse transcriptase and SYBR[®] Green⁶⁵.

An alternative explanation exists for the varied *TKTL1* expression between autistic and unaffected males between pedigrees. The variation could be due to an interaction between autism and family. *TKTL1* may be contributing to autism only in some families while in others it has little or no effect. The intersecting lines in the graph in Figure 3.6 demonstrate a potential interaction between autism and family. However, the interaction between a fixed and random variable cannot be tested for given the experimental design and statistical approach implemented in this study.

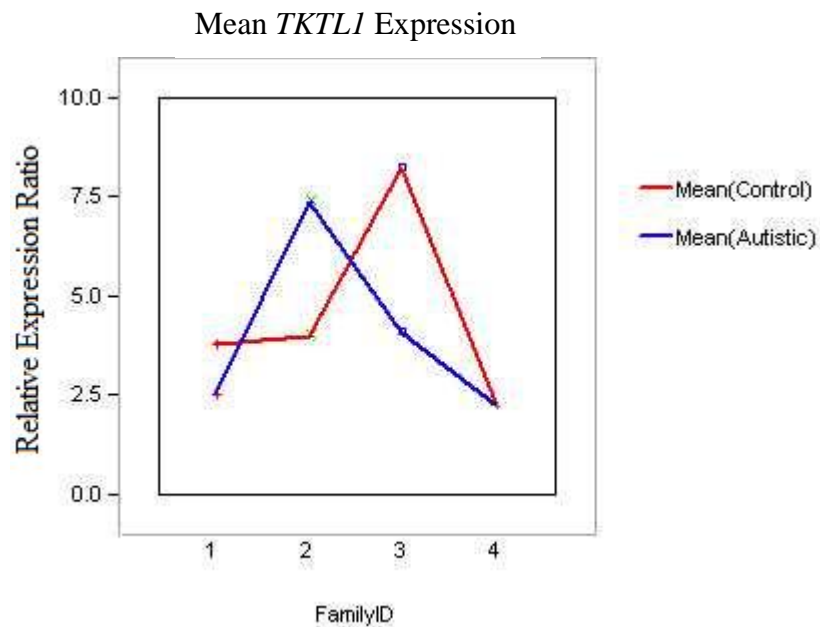


Figure 3.6 Graph depicting the autistic and control mean relative *TKTL1* expression ratio in each family. FamilyIDs: 1 = 74-0264, 2 = 61-3511, 3 = 63-156, 4 = 72-0890.

Chapter 4: Synopsis

Oxidative stress has been implicated in the pathogenesis of autism. The pentose phosphate pathway is responsible for combating oxidative stress by reducing glutathione, which subsequently reduces free radicals. Previous studies have shown a decreased GSH/GSSG ratio and an increased free radical generation in lymphoblastoid cells of autistic and unaffected individuals⁴⁵. Additionally, the amount of reduced glutathione in the cell is decreased when transaldolase is overexpressed⁴². Combined, there is reason to believe that *TKTL1* overexpression causes a decreased ability of the cell to reduce glutathione.

Overexpression of *TKTL1* in this study significantly decreased the GSH/GSSG ratio in the cell, indicating a heightened state of oxidative stress. It was thought that the NADPH/NADP⁺ ratio would decrease as well, however inconclusive results were obtained and further testing is required. *G6pdx* expression, however, did decrease upon *TKTL1* overexpression. The decrease of both the GSH/GSSG ratio and *G6pdx* expression lead me to hypothesize that the NADPH/NADP⁺ ratio actually decreases as well.

Skuse et al. suggested that an X-linked imprinted gene is involved in autism⁶⁰, leading us to analyze autistic and unaffected individuals for *TKTL1* expression differences. It was thought that *TKTL1* expression may be higher in autistic individuals because of its apparent effect on oxidative stress; however no conclusive deduction could be made about *TKTL1* expression differences between individuals.

Potential autism susceptibility genes have been analyzed directly in brain tissue using real-time RT-PCR⁶⁶. Since the brain is highly susceptible to the effects of oxidative stress, analysis of *TKTL1* expression in brain tissue would prove highly informative.

Chapter 5: Methods

Protocol 1: *TKTL1* Expression Construct Formation

The full-length human *TKTL1* CDS (Open Biosystems clone #4825931) was inserted into a pCAGGS vector (Supplemental Figure 1), which contains a chicken β -actin promoter. Both were digested with *EcoRI* and then ligated together with T4 DNA ligase as per standard methods. Successful construct formation was determined by *BamHI* digest and DNA sequencing. The hTktl1 primers used for sequencing can be found in Supplemental Table 1.

Protocol 2: Expression of *TKTL1*

The *TKTL1* expression construct (hTktl1-pCAGGS) was co-transfected with GFP-pCAGGS into HT-22 cells, a mouse hippocampal cell line. T75 flasks were seeded with 1×10^6 cells in 10mL of media (DMEM, 10% FBS, 1% L-glutamine, 1% penicillin/streptomycin) and incubated overnight at 37°C, 5% CO₂. A transfection mix was then prepared with 750 μ l DMEM, 3 μ l LipofectamineTM PLUSTM Reagent, 1 μ g GFP-pCAGGS and 1 μ g control (empty pCAGGS vector) or hTktl1-pCAGGS. This was incubated at room temperature for 5 minutes, then 9 μ l of LipofectamineTM LTX was added and this was incubated at room temperature for 30 minutes. The transfection mix was added to the T75 flasks along with 3mL of media (DMEM, 10% FBS, 1% L-glutamine) and incubated for 5 hours at 37°C, 5% CO₂. The media was then changed to the antibiotic-containing media above. The cells were incubated for 3 days, with a media

change on day 2. On day 3 the cells were imaged and harvested. The cells were harvested in ice cold 1x PBS using a rubber policeman. Cell pellets were stored at -80°C.

Protocol 3: Western Blot

Western blot was performed using cell pellets and established protocols. The primary antibody was a monoclonal mouse anti-human TKTL1 antibody (Abcam[®]). The secondary antibody was stabilized Peroxidase Conjugated Goat anti-Mouse (H + L) (Thermo Scientific). After blotting, proteins were detected using Western Lightning[®] Plus-ECL (PerkinElmer).

Protocol 4: Total RNA Extraction

Total RNA was extracted from cell pellets using the RNeasy Mini Kit (QIAGEN) as per manufacturer's instructions. The RNA was subsequently DNased using TURBO DNA-free[™] (Ambion[®]).

Protocol 5: Real-Time RT-PCR

cDNA synthesis was performed with 1µg of RNA using a qScript cDNA Synthesis kit (Quanta BioSciences, Inc.[™]) as per manufacturer's protocol. Real-time RT-PCR was performed using PerfeCTa[®] SYBR[®] Green FastMix[®] for iQ (Quanta BioSciences, Inc.[™]) and primers "AF TKTL1 F1" and "AF TKTL1 R1" for *TKTL1/Tktl1*, "G6pd F" and "G6pd R" for *G6pdx*, and "MF3" and "MR3" for mouse β-actin (Supplemental Table 1). The cycling conditions were as follows: 95°C for 3 min, 40 cycles of 95°C for 10 secs and 63.5°C (for *TKTL1/Tktl1*) or 63°C (for *G6pdx*) for 30 secs,

95°C for 1 min, 55°C for 1 min, 80 cycles of 55°C for 10 secs + 0.5°C/cycle.

Mathematical analysis of real-time RT-PCR data was carried out as described by normalizing and comparing C_t values of the genes of interest to β -actin⁶⁷.

Protocol 6: Glutathione Assay

Cell pellets were homogenized in the appropriate buffer and then deproteinized using metaphosphoric acid (Sigma-Aldrich®). Deproteinized samples were assayed with the Glutathione Assay Kit (Cayman Chemical). As per manufacturer's instructions, total GSH was detected via a colorimetric reaction with DTNB. GSSG was detected by addition of 2-vinylpyridine (Sigma-Aldrich®) prior to assaying. A 96-well plate reader was used to measure the absorbance at 405nm at 5 minute intervals over a period of 30 minutes. The 25 minute read was used for the end-point analysis. End point analysis: [(sample absorbance – standard y-intercept) / (standard slope)] * 2. All values were determined per manufacturer's protocol.

Protocol 7: NADP⁺/NADPH Assay

Cell pellets were homogenized in provided buffers from the EnzyChrom™ NADP⁺/NADPH Assay Kit (BioAssay Systems). As per manufacturer's protocol, NADP⁺ and NADPH were measured via a colorimetric reaction based on the ability of NADPH to reduce tetrazolium dye (MTT). A 96-well plate reader was used to measure the absorbance at 565nm at time “zero” and after a thirty minute incubation at room temperature. OD₀ was subtracted from OD₃₀ and the Δ OD was used to calculate the NADP⁺ and NADPH concentrations using the standard curve.

Protocol 8: Human Lymphoblastoid Cell Culture

Human lymphoblastoid cell lines were received from Rutgers University Cell and DNA Repository at Rutgers, The State University of New Jersey, per NIMH permission. The cell lines consisted of lymphoblasts from individuals affected with autism or ASD (as diagnosed by the DSM-IV) and unaffected siblings. The cell lines were received as 1mL aliquots cryopreserved in 45% RPMI-1640, 50% FBS and 5% DMSO.

10mL of fresh media (88% RPMI-1640, 10% FBS, 1% penicillin/streptomycin and 1% nonessential amino acids) was added to T-75 flasks. The cell lines were thawed at 37°C and pipetted into one flask each. 10mL of media was added to each flask 24 hours later. Fresh media was added as needed to maintain a cell density between 200,000 cells/mL and 500,000 cells/mL. Cells were collected as necessary.

When collected, the cell lines were either frozen down or stored as pellets. In both cases, the cell suspension was centrifuged at 1,000 x g for 5 minutes at 4°C and then the media was removed. To freeze down, the cells were resuspended in freezing media (90% media from above and 10% DMSO) and 1mL aliquots were stored in cryotubes in liquid nitrogen. The cell pellets were stored at -80°C.

Protocol 9: Human Lymphoblastoid Real-Time RT-PCR

Total RNA was extracted from the human lymphoblastoid cell pellets using TRIzol[®]. Subsequently cDNA was prepared as per manufacturer's protocol (qScript[™] cDNA Synthesis kit, Quanta BioSciences, Inc.[™]). Real-time PCR was performed using PerfeCTa[®] SYBR[®] Green FastMix[®] for iQ (Quanta BioSciences, Inc.[™]) as per usual methods using the primers "AF hTktl1 F14" and "AF hTktl1 R14" for *TKTL1* and

“hGAPDH F” and “hGAPDH R” for *GAPDH* (Supplemental Table 1). The cycling conditions were as follows: 95°C for 3 min, 40 cycles of 95°C for 10 secs and 63°C for 30 secs, 95°C for 1 min, 55°C for 1 min, 80 cycles of 55°C for 10 secs + 0.5°C/cycle. Mathematical analysis of the data was carried out as described by normalizing the C_t values of *TKTL1* to *GAPDH* and comparing the relative expression ratios⁶⁷.

Chapter 6: Supplemental Information

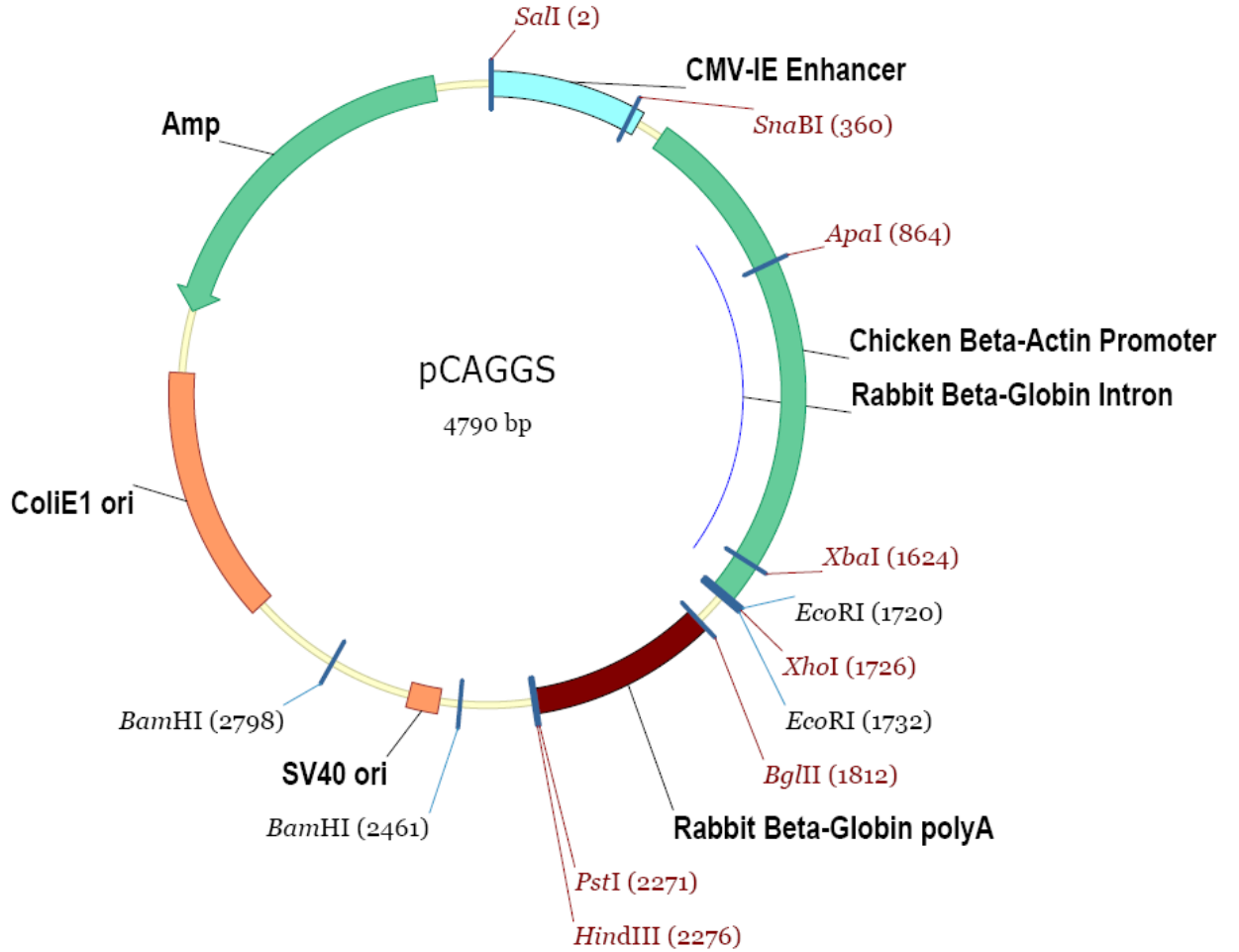
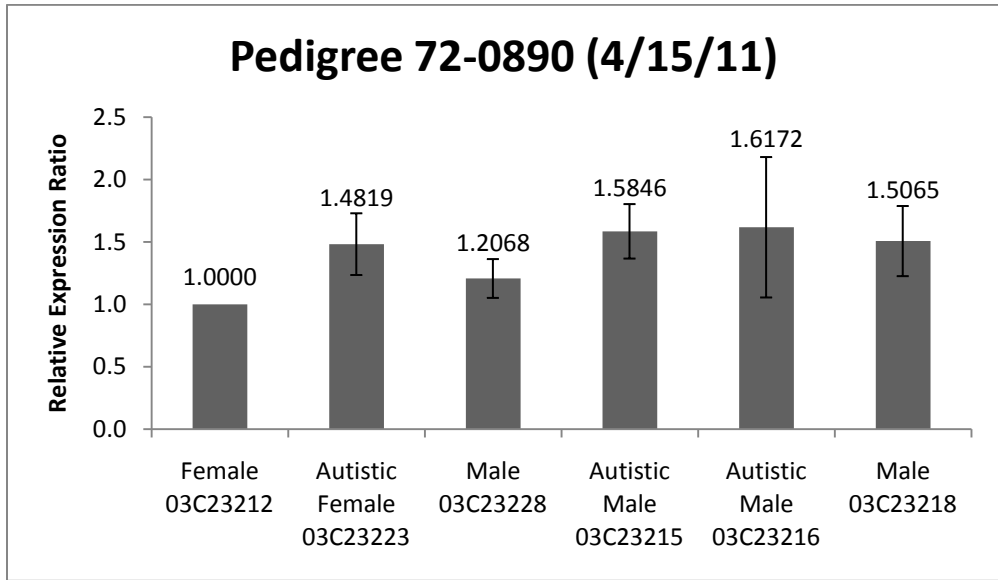
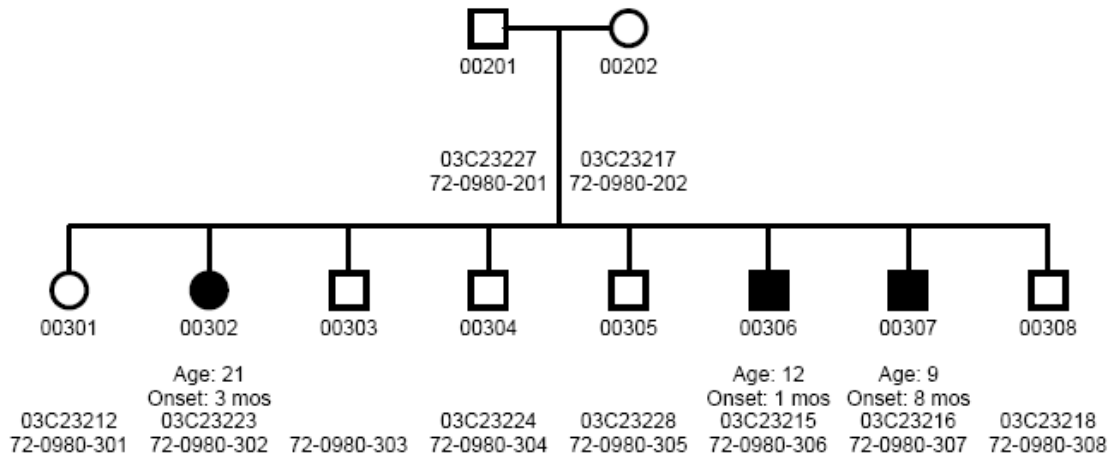


Figure 1 pCAGGS vector map. Commercially available expression vector used for *TKTL1* transfection into HT-22 cells. The *TKTL1* CDS was inserted at the *EcoRI* sites. Image provided by the LoTurco laboratory.

Pedigree 72-0890



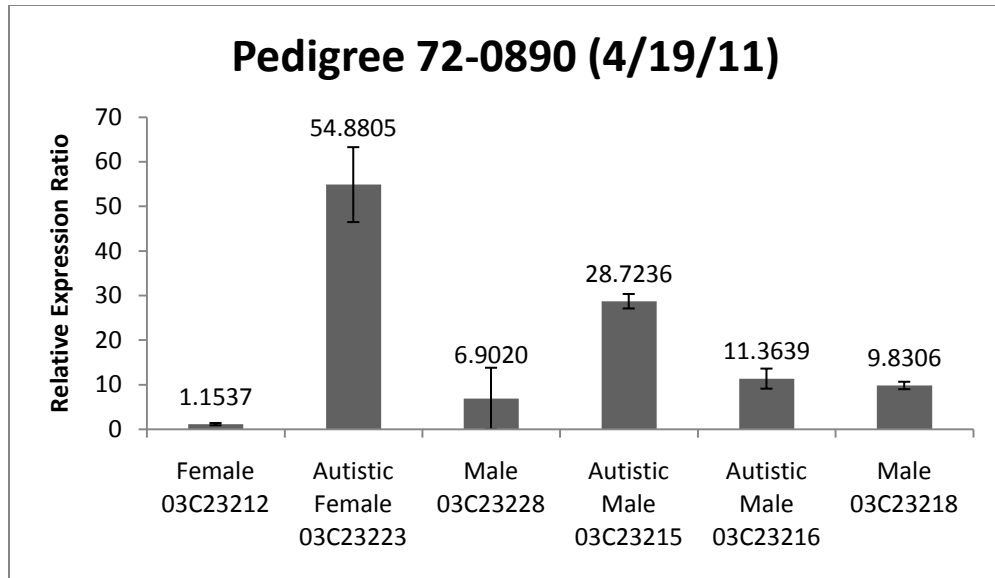
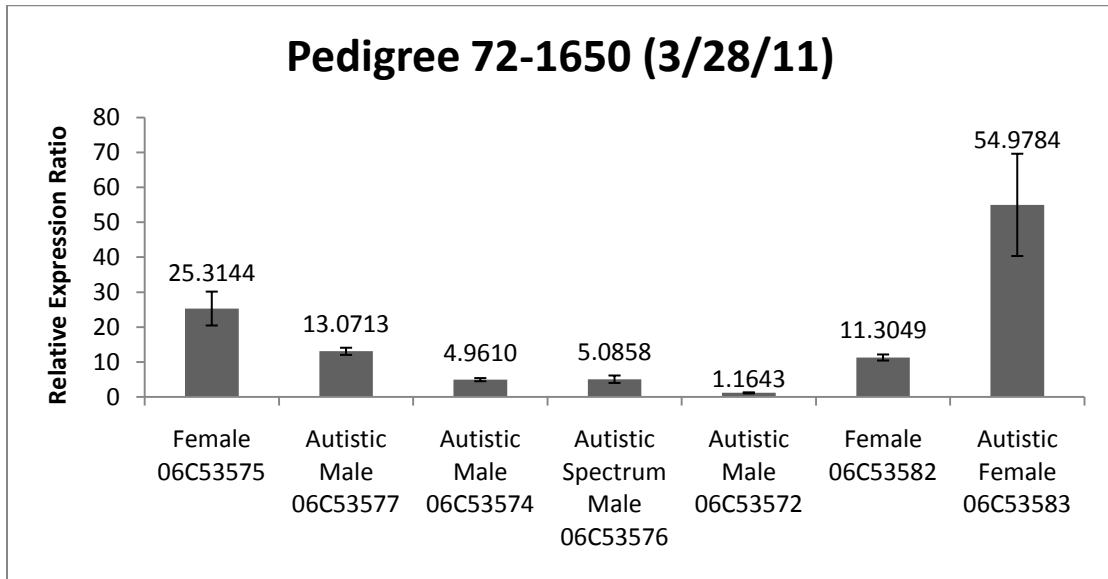
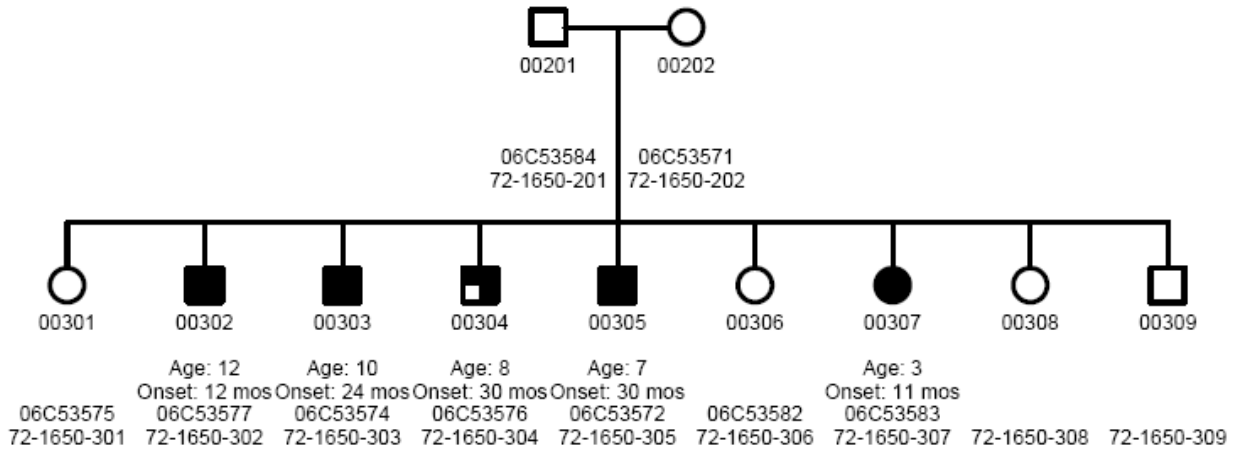


Figure 2 Two separate real-time RT-PCR trials of pedigree 72-0890. Error bars indicate a 95% confidence interval.

Pedigree 72-1650



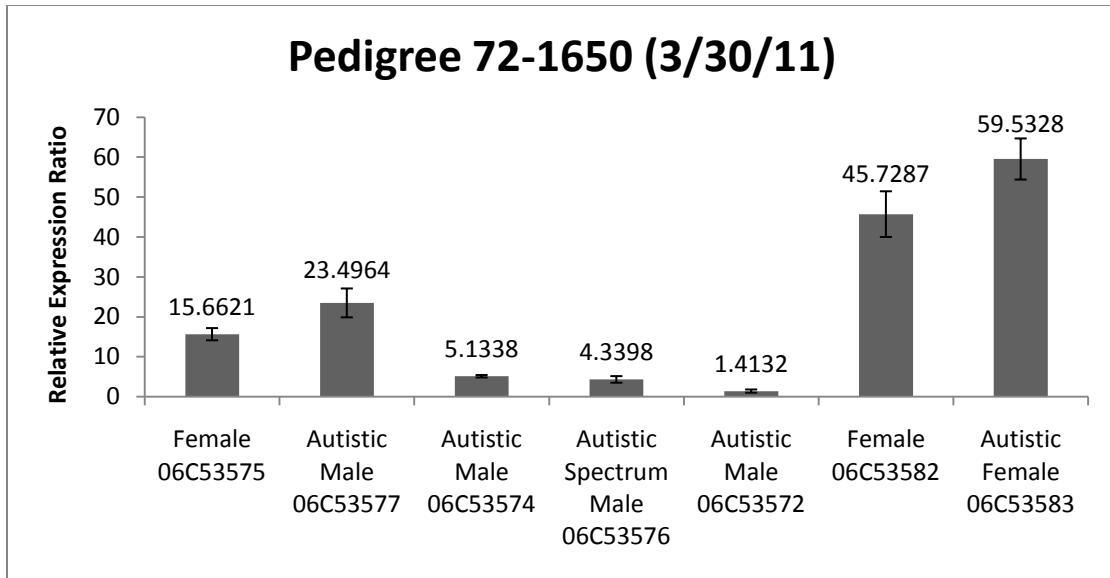


Figure 3 Two separate real-time RT-PCR trials for pedigree 72-1650. Error bars indicate a 95% confidence interval.

Pedigree 74-0264

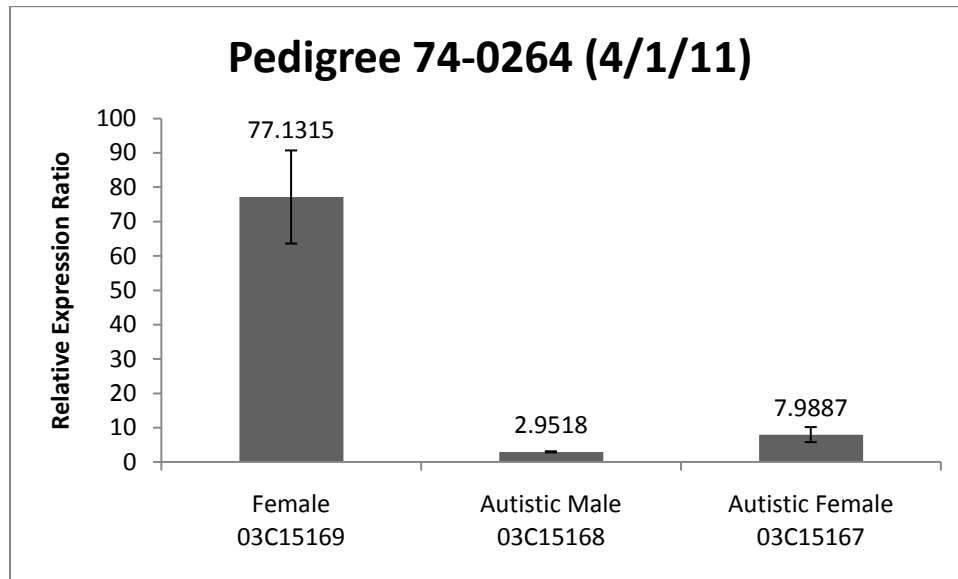
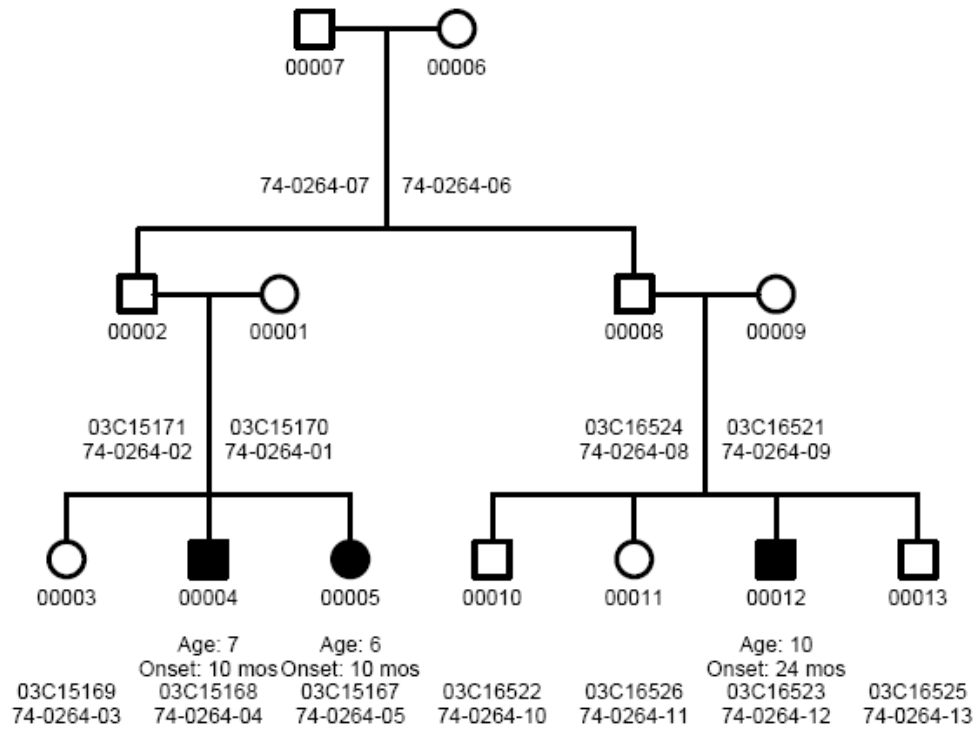


Figure 4 Real-time RT-PCR results for one trial of half of pedigree 74-0264. These individuals are cousins with the other half of this pedigree (shown below). Error bars indicate a 95% confidence interval.

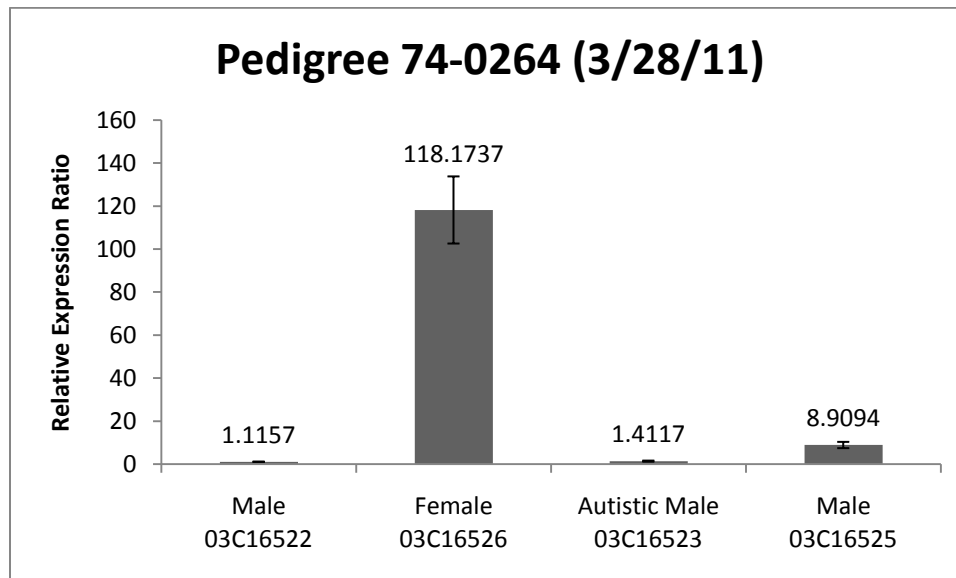
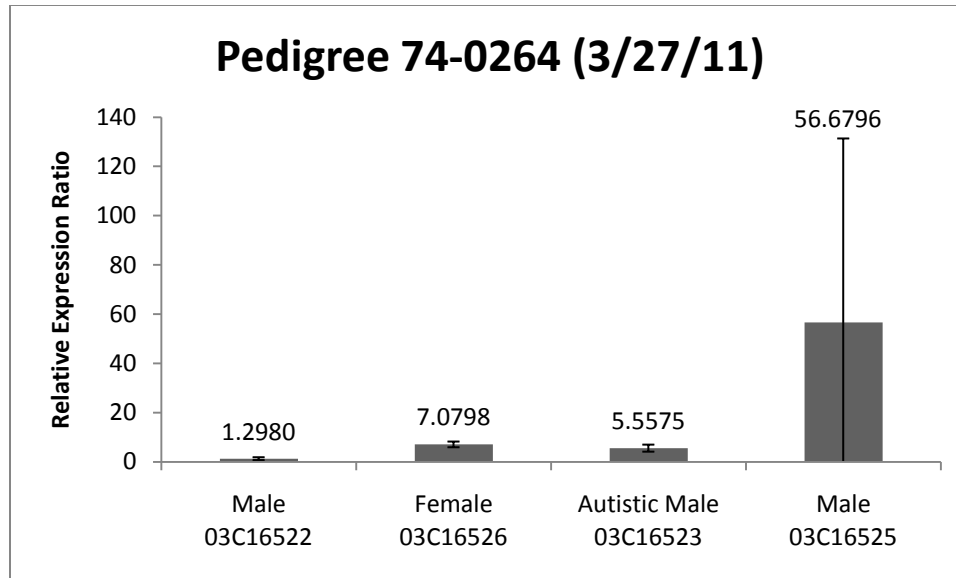
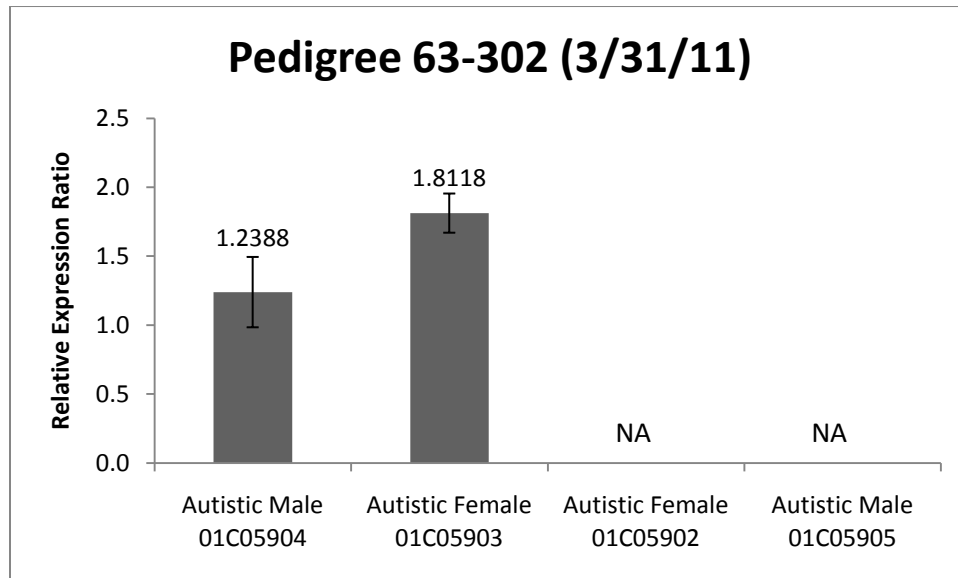
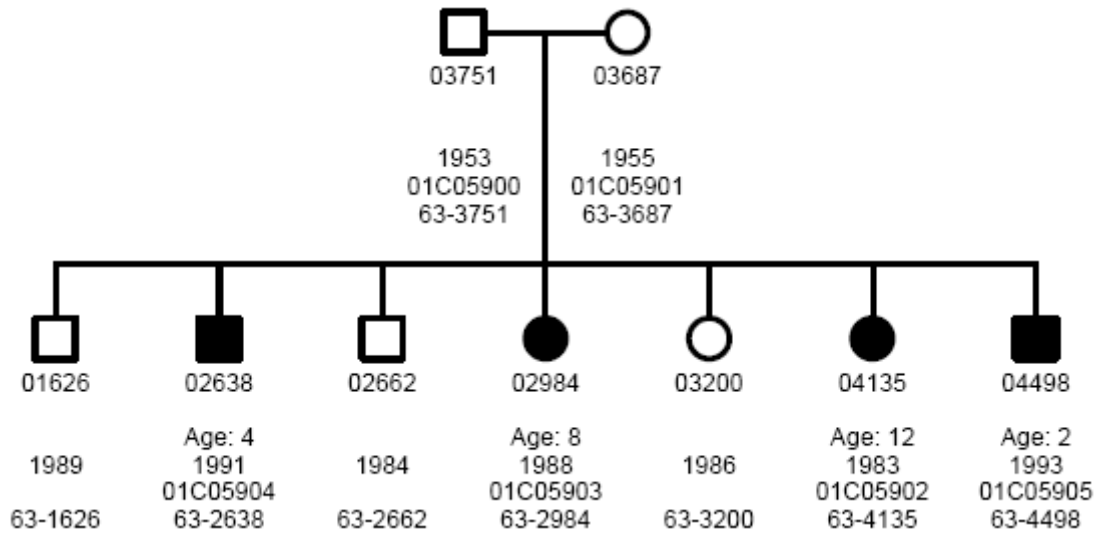


Figure 5 Real-time RT-PCR results for two separate trials of half of pedigree 74-0264. These individuals are cousins with the other half of this pedigree (shown above). Error bars indicate a 95% confidence interval.

Pedigree 63-302



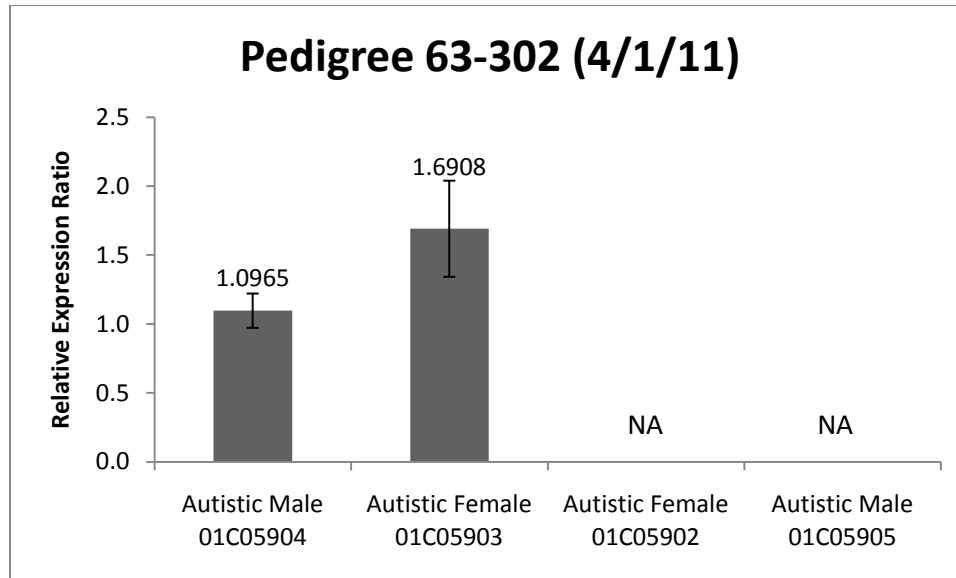
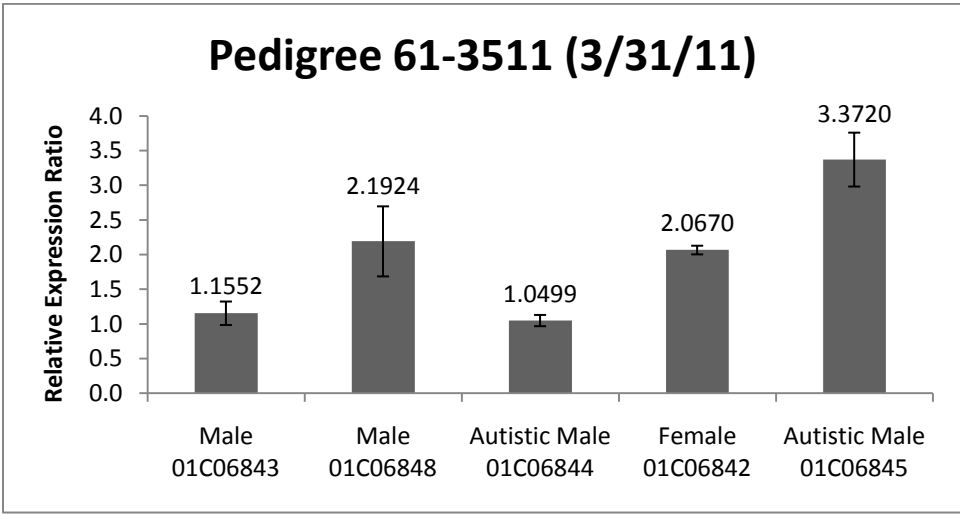
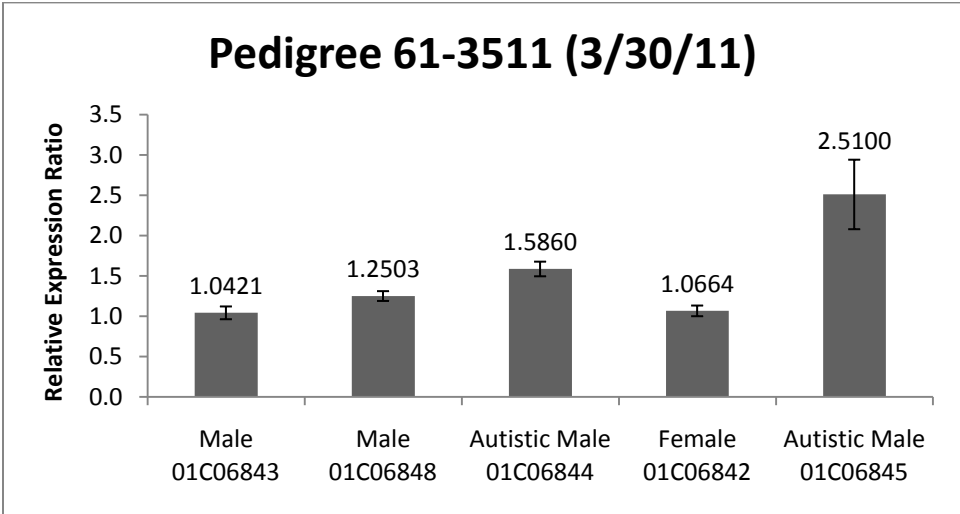
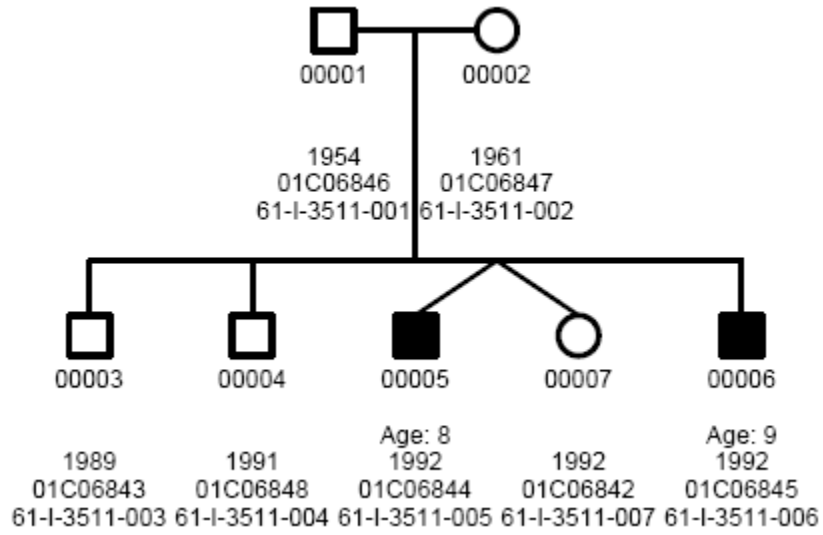


Figure 6 Real-time RT-PCR results for two separate trials of pedigree 63-302. Data was not available for Autistic Female 01C05902 and Autistic Male 01C05905. Error bars indicate a 95% confidence interval.

Pedigree 61-3511



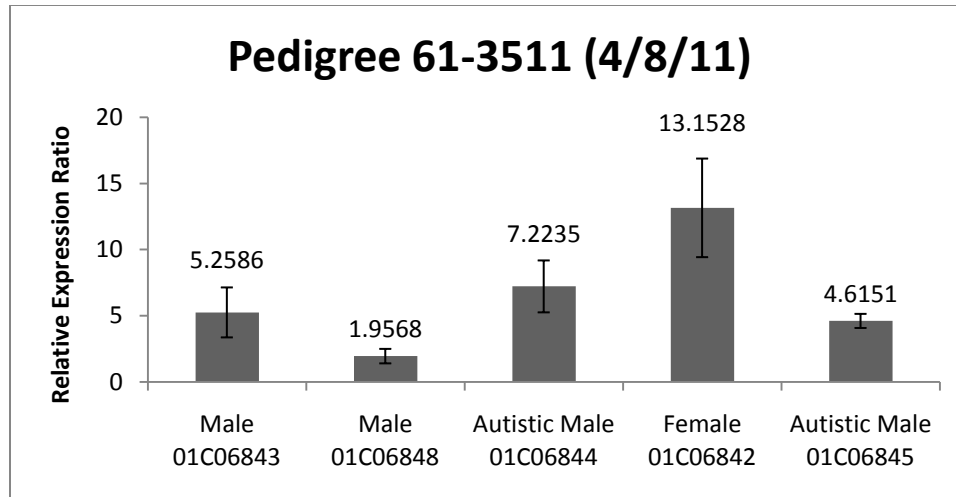
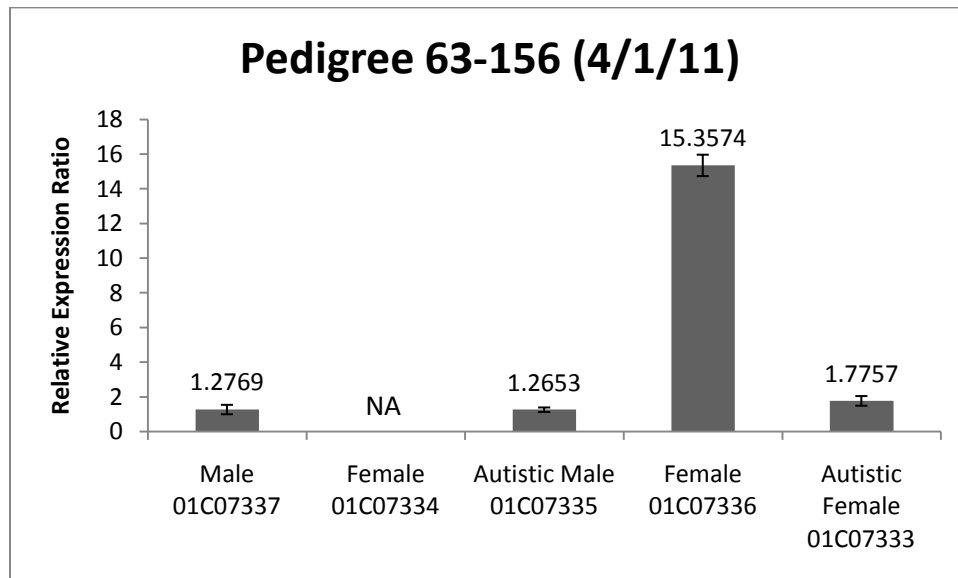
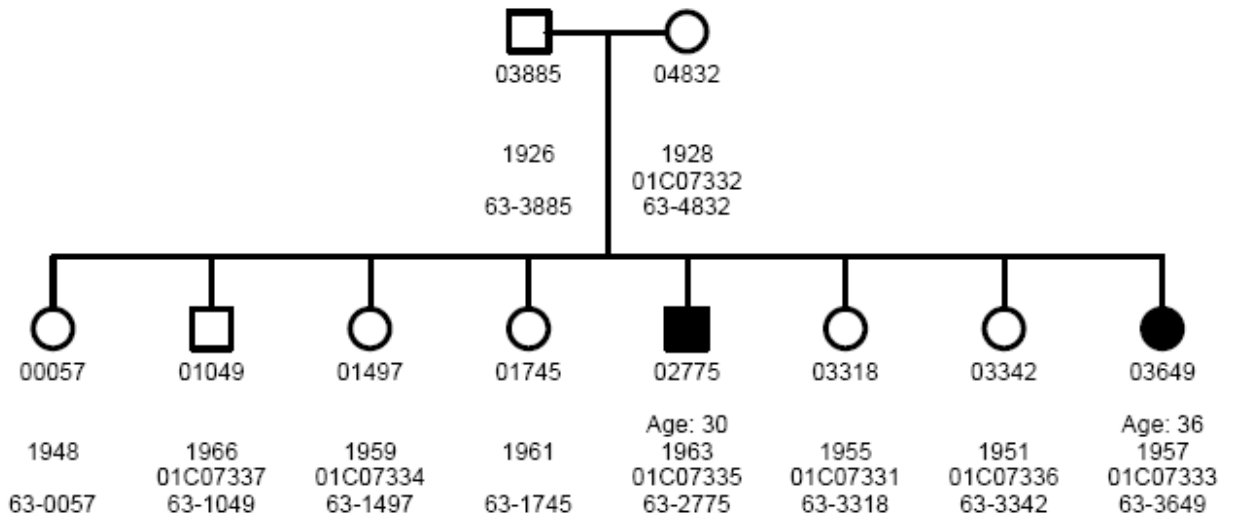


Figure 7 Real-time RT-PCR results for three separate trials of pedigree 61-3511. Error bars indicate a 95% confidence interval.

Pedigree 63-156



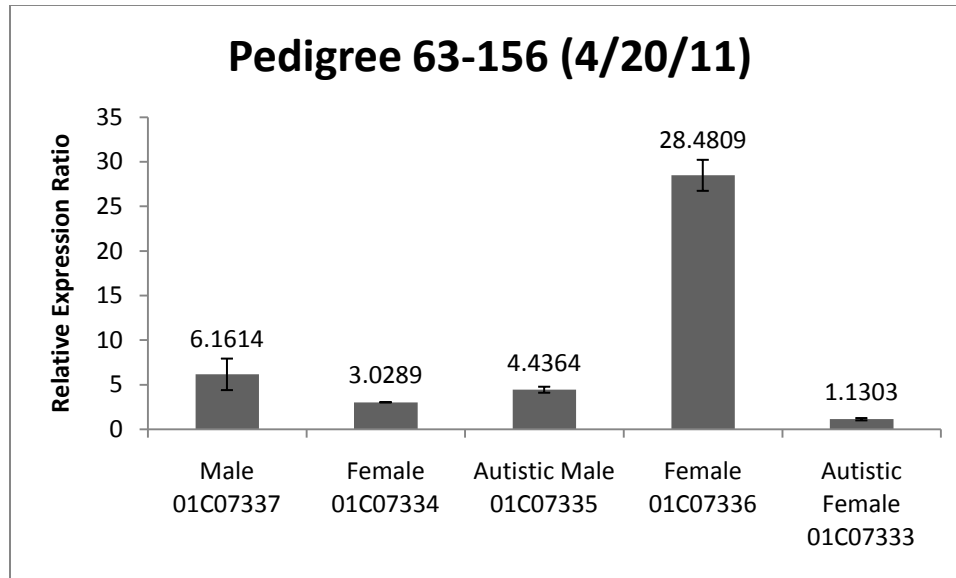


Figure 8 Real-time RT-PCR results for two separate trials of pedigree 63-156. Data was not available for Female 01C07334 on 4/1/11. Error bars indicate a 95% confidence interval.

Primer Name	Sequence (5'→ 3')	Gene
M13 F	CAGGAAACAGCTATGAC	Vector
M13 R	GTAAAACGACGGCCAG	Vector
AF pCAGGS F4	TTCAGACTCCAAAGGGGTTG	pCAGGS Vector
hTktl1 F7 (Operon)	ATGCCGAGAGAAAGAGCAGA	<i>TKTL1</i>
hTktl1 F7 (Invitrogen)	GCATATGCAAGTACCGCTCT	<i>TKTL1</i>
hTktl1 F11	GAGGCGAGGGCTGAGTTC	<i>TKTL1</i>
hTktl1 R3	AAACATAAACACAGGGTAAAGAGGC	<i>TKTL1</i>
hTktl1 R5	TTCTGAGGACTCGCCATCACTC	<i>TKTL1</i>
hTktl1 R10	TTCAATCCACATTTTCTTTACTCATG	<i>TKTL1</i>
hTktl1 R13	GGCATCTGCTCTTTCTCTCG	<i>TKTL1</i>
hTktl1 R15	AATTCCTCGGACTTCCCCT	<i>TKTL1</i>
hTktl1 R16	CGGATTCTCTGGATCTGACTG	<i>TKTL1</i>
Actb MF3	ACACCCGCCACCAGTTCG	β -Actin
Actb MR3	CGATGGAGGGGAATACAGCC	β -Actin
AF TKTL1 F1	ATGTGGCAACAGGATGGC	<i>TKTL1/Tktl1</i>
AF TKTL1 R1	TGGTCTGTATCTGGCTCTCAATTAA	<i>TKTL1/Tktl1</i>
G6pd F	AGCCTCCTATAAGCACCTCAACAGCC	<i>G6pdx</i>
G6pd R	TCCACGATGATGCGGTTCCAGC	<i>G6pdx</i>
hGAPDH F	AACTTTGGTATCGTGGAAGG	<i>GAPDH</i>
hGAPDH R	ACACGTTGGCAGTGGGGACA	<i>GAPDH</i>
AF hTktl1 F14	TCTGTCTGGGAGGCAATGGCC	<i>TKTL1</i>
AF hTktl1 R14	TCCCGGCCGTCCACCACATAA	<i>TKTL1</i>

Table 1 Name, sequence and gene for the primers used throughout the thesis.

Trial #	Control/Sample	Average GSH/GSSG	Standard Deviation
1	Control	NA	NA
	Sample	NA	NA
2	Control	NA	NA
	Sample	NA	NA
3	Control	7.32768	0.42949
	Sample	2.82402	0.15848
4	Control	NA	NA
	Sample	NA	NA
5	Control	NA	NA
	Sample	NA	NA
6	Control	8.95068	1.23647
	Sample	1.34007	0.12721
7	Control	1.23923	0.12119
	Sample	1.27867	0.21110
8	Control	9.14736	0.25454
	Sample	6.02062	0.21985
9	Control	3.49679	0.09919
	Sample	3.36254	0.11754

Table 2 Glutathione assay results. “NA” (Not Applicable) in the GSH/GSSG column means that the ratio could not be determined because the GSSG concentration was negative.

Trial #	Control/Sample	Average NADPH/NADP⁺	Standard Deviation
1	Control	0.67111	0.25864
	Sample	0.90285	0.04089
2	Control	1.03492	0.19806
	Sample	0.51953	0.06389
3	Control	5.37500	NA
	Sample	0.79070	NA
4	Control	0.62909	0.02542
	Sample	0.46992	0.02570
5	Control	0.23906	0.02241
	Sample	0.30233	NA

Table 3 NADP⁺/NADPH assay results. “NA” indicates that the standard deviation could not be calculated because only one sample in the triplicate provided usable data.

Chapter 7: References

1. Bartolomei, M.S. Genomic imprinting: employing and avoiding epigenetic processes. *Genes Dev* **23**, 2124-2133 (2009).
2. Weaver, J.R., Susiarjo, M. & Bartolomei, M.S. Imprinting and epigenetic changes in the early embryo. *Mamm. Genome* **20**, 532-543 (2009).
3. Aapola, U. et al. Isolation and initial characterization of a novel zinc finger gene, DNMT3L, on 21q22.3, related to the cytosine-5-methyltransferase 3 gene family. *Genomics* **65**, 293-298 (2000).
4. Bourc'his, D., Xu, G.L., Lin, C.S., Bollman, B. & Bestor, T.H. Dnmt3L and the establishment of maternal genomic imprints. *Science* **294**, 2536-2539 (2001).
5. Yokomine, T., Hata, K., Tsudzuki, M. & Sasaki, H. Evolution of the vertebrate DNMT3 gene family: a possible link between existence of DNMT3L and genomic imprinting. *Cytogenet. Genome Res* **113**, 75-80 (2006).
6. Brinkman, A.B. et al. Histone modification patterns associated with the human X chromosome. *EMBO Rep* **7**, 628-634 (2006).
7. Vakoc, C.R., Sachdeva, M.M., Wang, H. & Blobel, G.A. Profile of Histone Lysine Methylation across Transcribed Mammalian Chromatin. *Mol Cell Biol* **26**, 9185-9195 (2006).
8. Ruiz-Carrillo, A. & Jorcano, J.L. An octamer of core histones in solution: central role of the H3-H4 tetramer in the self-assembly. *Biochemistry* **18**, 760-768 (1979).
9. Bartolomei, M.S. Genomic imprinting: employing and avoiding epigenetic processes. *Genes Dev* **23**, 2124-2133 (2009).
10. Bartolomei, M.S., Zemel, S. & Tilghman, S.M. Parental imprinting of the mouse H19 gene. *Nature* **351**, 153-155 (1991).
11. DeChiara, T.M., Robertson, E.J. & Efstratiadis, A. Parental imprinting of the mouse insulin-like growth factor II gene. *Cell* **64**, 849-859 (1991).
12. Ferguson-Smith, A.C., Cattanach, B.M., Barton, S.C., Beechey, C.V. & Surani, M.A. Embryological and molecular investigations of parental imprinting on mouse chromosome 7. *Nature* **351**, 667-670 (1991).
13. Leighton, P.A., Saam, J.R., Ingram, R.S., Stewart, C.L. & Tilghman, S.M. An enhancer deletion affects both H19 and Igf2 expression. *Genes & Development* **9**, 2079 -2089 (1995).
14. Thorvaldsen, J.L., Duran, K.L. & Bartolomei, M.S. Deletion of the H19 differentially methylated domain results in loss of imprinted expression of H19 and Igf2. *Genes Dev* **12**, 3693-3702 (1998).
15. Thorvaldsen, J.L., Mann, M.R.W., Nwoko, O., Duran, K.L. & Bartolomei, M.S. Analysis of sequence upstream of the endogenous H19 gene reveals elements both essential and dispensable for imprinting. *Mol. Cell. Biol* **22**, 2450-2462 (2002).
16. Bell, A.C., West, A.G. & Felsenfeld, G. The protein CTCF is required for the enhancer blocking activity of vertebrate insulators. *Cell* **98**, 387-396 (1999).
17. Bell, A.C. & Felsenfeld, G. Methylation of a CTCF-dependent boundary controls imprinted expression of the Igf2 gene. *Nature* **405**, 482-485 (2000).
18. Koerner, M.V., Pauler, F.M., Huang, R. & Barlow, D.P. The function of non-coding RNAs in genomic imprinting. *Development* **136**, 1771-1783 (2009).

19. Braidotti, G. et al. The Air noncoding RNA: an imprinted cis-silencing transcript. *Cold Spring Harb. Symp. Quant. Biol* **69**, 55-66 (2004).
20. Glaser, R.L., Ramsay, J.P. & Morison, I.M. The imprinted gene and parent-of-origin effect database now includes parental origin of de novo mutations. *Nucleic Acids Res* **34**, D29-31 (2006).
21. Monkhorst, K., Jonkers, I., Rentmeester, E., Grosveld, F. & Gribnau, J. X inactivation counting and choice is a stochastic process: evidence for involvement of an X-linked activator. *Cell* **132**, 410-421 (2008).
22. Chadwick, L.H., Pertz, L.M., Broman, K.W., Bartolomei, M.S. & Willard, H.F. Genetic control of X chromosome inactivation in mice: definition of the Xce candidate interval. *Genetics* **173**, 2103-2110 (2006).
23. Brown, C.J. et al. A gene from the region of the human X inactivation centre is expressed exclusively from the inactive X chromosome. *Nature* **349**, 38-44 (1991).
24. Lee, J.T., Davidow, L.S. & Warshawsky, D. Tsix, a gene antisense to Xist at the X-inactivation centre. *Nat. Genet* **21**, 400-404 (1999).
25. Raefski, A.S. & O'Neill, M.J. Identification of a cluster of X-linked imprinted genes in mice. *Nat Genet* **37**, 620-624 (2005).
26. Schenk, G., Duggleby, R.G. & Nixon, P.F. Properties and functions of the thiamin diphosphate dependent enzyme transketolase. *Int. J. Biochem. Cell Biol* **30**, 1297-1318 (1998).
27. Ueki, T., Uyama, T., Yamamoto, K., Kanamori, K. & Michibata, H. Exclusive expression of transketolase in the vanadocytes of the vanadium-rich ascidian, *Ascidia sydneiensis samea*. *Biochim. Biophys. Acta* **1494**, 83-90 (2000).
28. Esposito, M. et al. Human Transaldolase and Cross-Reactive Viral Epitopes Identified by Autoantibodies of Multiple Sclerosis Patients. *J Immunol* **163**, 4027-4032 (1999).
29. Vatanaviboon, P., Varaluksit, T., Seeanukun, C. & Mongkolsuk, S. Transaldolase exhibits a protective role against menadione toxicity in *Xanthomonas campestris* pv. *phaseoli*. *Biochem. Biophys. Res. Commun* **297**, 968-973 (2002).
30. Du, M.X. et al. Identification of novel small-molecule inhibitors for human transketolase by high-throughput screening with fluorescent intensity (FLINT) assay. *J Biomol Screen* **9**, 427-433 (2004).
31. Coy, J.F., Dressler, D., Wilde, J. & Schubert, P. Mutations in the transketolase-like gene TKTL1: clinical implications for neurodegenerative diseases, diabetes and cancer. *Clin. Lab* **51**, 257-273 (2005).
32. Pannunzio, P., Hazell, A.S., Pannunzio, M., Rao, K.V. & Butterworth, R.F. Thiamine deficiency results in metabolic acidosis and energy failure in cerebellar granule cells: an in vitro model for the study of cell death mechanisms in Wernicke's encephalopathy. *J. Neurosci. Res* **62**, 286-292 (2000).
33. Paoletti, F., Mocali, A., Marchi, M., Sorbi, S. & Piacentini, S. Occurrence of transketolase abnormalities in extracts of foreskin fibroblasts from patients with Alzheimer's disease. *Biochem. Biophys. Res. Commun* **172**, 396-401 (1990).
34. Zhao, J. & Zhong, C.-J. A review on research progress of transketolase. *Neurosci Bull* **25**, 94-99 (2009).
35. Hammes, H.-P. et al. Benfotiamine blocks three major pathways of hyperglycemic damage and prevents experimental diabetic retinopathy. *Nat. Med* **9**, 294-299 (2003).

36. Boros, L.G. et al. Oxythiamine and dehydroepiandrosterone inhibit the nonoxidative synthesis of ribose and tumor cell proliferation. *Cancer Res* **57**, 4242-4248 (1997).
37. Langbein, S. et al. Expression of transketolase TKTL1 predicts colon and urothelial cancer patient survival: Warburg effect reinterpreted. *Br J Cancer* **94**, 578-585 (2006).
38. Coy, J.F. et al. Molecular cloning of tissue-specific transcripts of a transketolase-related gene: implications for the evolution of new vertebrate genes. *Genomics* **32**, 309-316 (1996).
39. Glinsky, G.V., Ivanova, Y.A. & Glinskii, A.B. Common malignancy-associated regions of transcriptional activation (MARTA) in human prostate, breast, ovarian, and colon cancers are targets for DNA amplification. *Cancer Lett* **201**, 67-77 (2003).
40. Glinsky, G.V., Krones-Herzig, A. & Glinskii, A.B. Malignancy-associated regions of transcriptional activation: gene expression profiling identifies common chromosomal regions of a recurrent transcriptional activation in human prostate, breast, ovarian, and colon cancers. *Neoplasia* **5**, 218-228 (2003).
41. Xu, X., Zur Hausen, A., Coy, J.F. & Löchelt, M. Transketolase-like protein 1 (TKTL1) is required for rapid cell growth and full viability of human tumor cells. *Int. J. Cancer* **124**, 1330-1337 (2009).
42. Banki, K., Hutter, E., Colombo, E., Gonchoroff, N.J. & Perl, A. Glutathione levels and sensitivity to apoptosis are regulated by changes in transaldolase expression. *J. Biol. Chem* **271**, 32994-33001 (1996).
43. Söğüt, S. et al. Changes in nitric oxide levels and antioxidant enzyme activities may have a role in the pathophysiological mechanisms involved in autism. *Clin. Chim. Acta* **331**, 111-117 (2003).
44. Zoroglu, S.S. et al. Increased oxidative stress and altered activities of erythrocyte free radical scavenging enzymes in autism. *Eur Arch Psychiatry Clin Neurosci* **254**, 143-147 (2004).
45. James, S.J. et al. Cellular and mitochondrial glutathione redox imbalance in lymphoblastoid cells derived from children with autism. *FASEB J* **23**, 2374-2383 (2009).
46. Ng, F., Berk, M., Dean, O. & Bush, A.I. Oxidative stress in psychiatric disorders: evidence base and therapeutic implications. *Int. J. Neuropsychopharmacol* **11**, 851-876 (2008).
47. Meguid, N.A., Dardir, A.A., Abdel-Raouf, E.R. & Hashish, A. Evaluation of Oxidative Stress in Autism: Defective Antioxidant Enzymes and Increased Lipid Peroxidation. *Biol Trace Elem Res* (2010).doi:10.1007/s12011-010-8840-9
48. Chauhan, A. & Chauhan, V. Oxidative stress in autism. *Pathophysiology* **13**, 171-181 (2006).
49. Bertoglio, K., Jill James, S., Deprey, L., Brule, N. & Hendren, R.L. Pilot study of the effect of methyl B12 treatment on behavioral and biomarker measures in children with autism. *J Altern Complement Med* **16**, 555-560 (2010).
50. Fradin, D. et al. Parent-of-origin effects in autism identified through genome-wide linkage analysis of 16,000 SNPs. *PLoS ONE* **5**, (2010).
51. Muhle, R., Trentacoste, S.V. & Rapin, I. The genetics of autism. *Pediatrics* **113**, e472-486 (2004).

52. Vorstman, J.A.S. et al. Identification of novel autism candidate regions through analysis of reported cytogenetic abnormalities associated with autism. *Mol. Psychiatry* **11**, 1, 18-28 (2006).
53. Cantor, R.M. Molecular genetics of autism. *Curr Psychiatry Rep* **11**, 137-142 (2009).
54. Schanen, N.C. Epigenetics of autism spectrum disorders. *Hum. Mol. Genet.* **15**, R138-150 (2006).
55. Depienne, C. et al. Screening for genomic rearrangements and methylation abnormalities of the 15q11-q13 region in autism spectrum disorders. *Biol. Psychiatry* **66**, 349-359 (2009).
56. Abrahams, B.S. & Geschwind, D.H. Advances in autism genetics: on the threshold of a new neurobiology. *Nat Rev Genet* **9**, 341-355 (2008).
57. Ma, D. et al. A genome-wide association study of autism reveals a common novel risk locus at 5p14.1. *Ann. Hum. Genet* **73**, 263-273 (2009).
58. Lu, A.T.-H. & Cantor, R.M. Allowing for sex differences increases power in a GWAS of multiplex Autism families. *Mol Psychiatry* (2010).doi:10.1038/mp.2010.127
59. Skuse, D.H. Imprinting, the X-chromosome, and the male brain: explaining sex differences in the liability to autism. *Pediatr. Res* **47**, 9-16 (2000).
60. Skuse, D.H. et al. Evidence from Turner's syndrome of an imprinted X-linked locus affecting cognitive function. *Nature* **387**, 705-708 (1997).
61. Creswell, C.S. & Skuse, D.H. Autism in association with Turner syndrome: Genetic implications for male vulnerability to pervasive developmental disorders. *Neurocase: The Neural Basis of Cognition* **5**, 511 (1999).
62. Baron-Cohen, S. The extreme male brain theory of autism. *Trends Cogn. Sci. (Regul. Ed.)* **6**, 248-254 (2002).
63. Tatton, W.G. et al. Glyceraldehyde-3-phosphate dehydrogenase in neurodegeneration and apoptosis signaling. *J. Neural Transm. Suppl* 77-100 (2000).
64. de Brouwer, A.P.M., Hans van Bokhoven & Kremer, H. Comparison of 12 Reference Genes for Normalization of Gene Expression Levels in Epstein-Barr Virus-Transformed Lymphoblastoid Cell Lines and Fibroblasts. at <<http://uconn.library.ingentaconnect.com/content/adis/mdt/2006/00000010/00000003/art00006>>
65. Bustin, S.A. Quantification of mRNA using real-time reverse transcription PCR (RT-PCR): trends and problems. *J. Mol. Endocrinol* **29**, 23-39 (2002).
66. Weiss, L.A. & Arking, D.E. A genome-wide linkage and association scan reveals novel loci for autism. *Nature* **461**, 802-808 (2009).
67. Pfaffl, M.W. A new mathematical model for relative quantification in real-time RT-PCR. *Nucleic Acids Res.* **29**, e45 (2001).